Implementation and validation of a Regional Climate Model for Bolivia

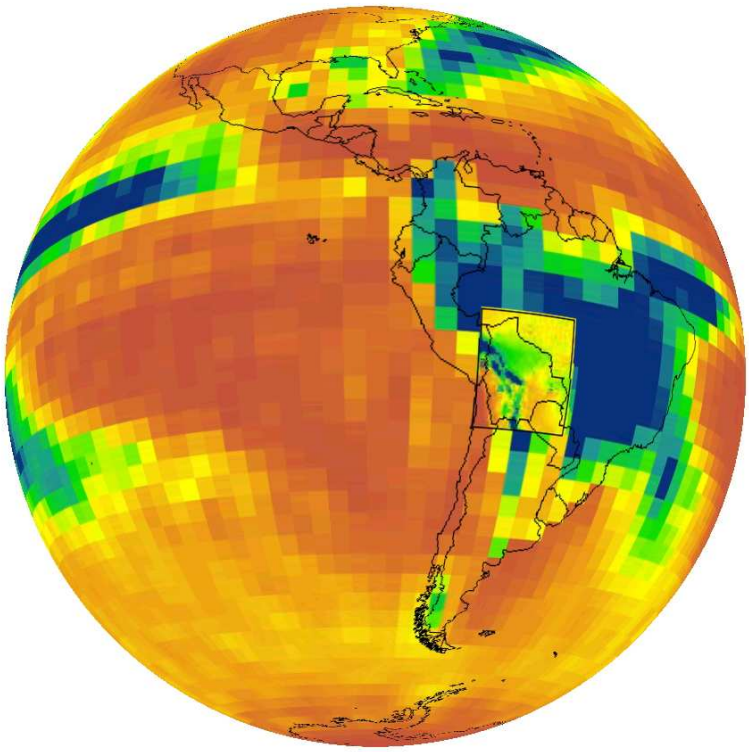

Version 1.2

July 2009,
Christian Seiler, Fundación Amigos de la Naturaleza (FAN-Bolivia)

Table of content

LIST OF FIGURES

LIST OF TABLES

ACRONYMS

DEM	Digital Elevation Model
ECHAM4	Global Circulation Model (Max Planck)
ECMWF	Centre for Medium-Range Weather Forecasts
ENSO	El Niño/Northern Oscilliation
ERA40	Re-analysis of meteorological observations
FAN-Bolivia	Fundación Amigos de la Naturaleza
FSUNRSM	Florida State Nested Regional Spectral Model
GCM	Global Circulation Model
GISSRCM	GISS Regional Climate Model
HadAM3P	Global Circulation Model (Hadley Centre)
HadCM3Q	Global Circulation Model (Hadley Centre)
ITCZ	Intertropical Convergence Zone
LBC	Lateral Boundary Condition
MOSES	Met Office Surface Exchange Scheme
OBS	Observations
PRECIS	Providing Regional Climates for Impact Studies
RCA3	Rossby Centre Regional Climate Model
RCM	Regional Climate Model
RegCM2	IRI Regional Climate Model
RMS	Root Mean Square Error
RSM	ECPS Regional Spectral Model
SACZ	South Atlantic Convergence Zone
SAMS	South American Monsoon System
SENAMHI	National Service of Meteorology and Hydrology
SPCZ	South Pacific Convergence Zone
SRES	Special Report on Emission Scenarios
SST	Sea Surface Temperature

ABSTRACT

A regional climate model is implemented and validated for Bolivia. Simulated monthly mean air temperature and precipitation are compared to meteorological observations. Modeled and observed data show similar seasonal cycles and are spatially correlated. With respect to temperature, the model estimates correct values in the lowlands but systematically underestimates temperature in the sub-Andean mountain range and in the highlands. With respect to precipitation, the model estimates significantly different values in the lowlands and systematically overestimates precipitation in the sub-Andean mountain range and in the highlands. Future climates maintain the basic seasonal temperature and precipitation cycle. However, future air temperature is expected to increase throughout Bolivia with more extreme changes in the highlands and the Amazon. Temperature is likely to increase by 1-2°C by 2030 and by 5-6°C by 2100, compared to the mean temperature of 1961-1990. Changes in precipitation are more complex. The lowlands show a more intense precipitation cycle with more precipitation during the rain- and less during the dry season (DJF and JJA respectively). Extreme relative changes include +53% and -36% by 2100. This more intense cycle is also visible in the Sub-Andean mountain range with strongest precipitation decreases around August. In the highlands, this pattern reverses by 2100 with strongest relative precipitation in-and decrease during the dry- and wet season respectively. Because of the high uncertainty of the spatial observed precipitation data, an improvement of the data with remote sensing images is recommendable. Furthermore, a review of the applicability of the model for the Andes is necessary. The author recommends analyzing the model's surface elevation and the parameterization of precipitation. If improvements are not feasible, the application of an alternative model must be considered.

***Key words*:** regional climate modeling; dynamical downscaling; statistical validation; climate change scenarios; surface climatology; Bolivia

1 Introduction

1.1 Motivation

The Bolivian NGO for nature conservation FAN-Bolivia and the Bolivian state department of Santa Cruz are jointly conducting a five year lasting pilot project on the adaptation of climate change (Programa Piloto Departamental de Adaptación al Cambio Climático). To explore possible climate change impacts, the project demands detailed and validated climate change projections for Bolivia. This report documents the implementation, analysis and validation of a Regional Climate Model for the Bolivian territory for climate change prediction purposes. The following chapters include a brief review on climate models, South America's basic climatology and the implementation, analysis and validation of a RCM for the Bolivian territory. Model outputs are analyzed with respect to monthly mean air temperature and monthly precipitation. Climate change scenarios are presented and compared to observed tendencies. Main findings are discussed and recommendations for further research are given.

1.2 Climate Models

Global Circulation Models (GCM) are mathematical representations of the earth's climate system. GCM couple processes related to the atmo-, hydro-, cryo- and biosphere and present highly complex and non-linear systems. Due to limited computing capacity, processes need to be simplified and represented at coarse spatial scales of about 250x250km. To increase the spatial resolution, GCM-results can be statistically or dynamically downscaled. The latter implies the application of a Regional Climate Model (RCM) and allows for spatial resolutions of few kilometers. Several RCM have been applied to South America in the recent past for process or predictability studies. Among them are RSM, FSUNRSM, GISSRCM and RegCM2 (Roads *et al*., 2003), RegCM3 (Seth *et al*., 2007), REMO (Silvestri *et al.,* 2009), RCA3 (Sörrensson *et al*., 2009) and PRECIS (Urrutia *et al*., 2009; Marengo *et al*., 2009) (Table 8). Only the latter three experiments with RCA3 and PRECIS include climate change predictions. Authors find reasonable spatial and temporal temperature and precipitation patterns; bias however, does exist. Models tend to overestimate precipitation in the Bolivian Andes. Mean

differences between modeled and observed seasonal temperature and precipitation include -2°C to +4°C and -100% to +100% respectively in Bolivia (Silvestri *et al.,* 2009). Future climates show an increase of temperature and an intensification of the precipitation cycle. Authors find a strong increase of air temperature in parts of the Amazon, accompanied by a decrease of temperature. A similar tendency for some parts of the Bolivian Andes is modeled.
Despite the existence of RCM-results for South America, a RCM is implemented explicitly for the Bolivian territory. This enables the author the full access to all data, an increase of the spatial resolution to approximately 25x25km, and the opportunity to test the performance a variety of different lateral boundary conditions (see chapter 2.5.1). Furthermore, the follow-up research aims at modeling interactions among climate, vegetation and deforestation, which demands for the full access to a RCM.

1.3 Atmospheric circulation of South America

Important components of South America's climatology include (*i*) the mountain ranges of the Andes and the Brazilian plateau, (*ii*) the high pressure cells in the SE-Pacific and SW-Atlantic, (*iii*) the Humboldt Current and (i*v*) the three main precipitation fields Intertropical Convergence Zone (ITCZ), South Atlantic Convergence Zone (SACZ) and South Pacific Convergence Zone (SPCZ) (Garreaud *et al.,* 2008).

Precipitation fields

The ITCZ is a belt of low pressure fields located along the equator. Here, trade winds from the northern and southern hemisphere converge, producing deep moist convection and hence large amounts of precipitation. The position of the ITCZ responds to the latitudinal shift of surface heating by the sun, but also depends on land-sea distribution, continental topography and Sea Surface Temperature (SST). The latitudinal shifts of the ITCZ lead to seasonal precipitation cycles with most precipitation during JJA in the north and during DJF in the south. The northern and southern extreme extensions of the ITCZ form southern Central America and central Argentina respectively (Veblen *et al.,* 2007). This migration of precipitation is recently referred to as the South American Monsoon System (SAMS) (Vera *et al*., 2006). Another feature of SAMS presents the second main precipitation field SACZ. SACZ is a diagonal band of all-year-round precipitation maxima expanding from the central part of the continent to the SW-Atlantic. The third main precipitation field SPCZ reaches the continent between its southern tip and 40°S. Here, a low-level westerly flow prevails throughout the year, leading to high precipitation at the western slopes and dry conditions east of the Andes (Garreaud *et al.,* 2008).

Wind fields

Driven by the high pressure cell in the SW-Atlantic, the easterly trade winds penetrate into the continent throughout the year and turn south when converge near the Andes. During the austral summer (DJF), a low pressure cell forms over the Chaco region ("Chaco low") (25°S), forcing the easterly trade winds to transport moisture from the Amazon to subtropical plains (35°S) by a low level jet. During the same time the upper-level high pressure cell "Bolivian High" forms over the Altiplano, favoring the transport of continental, moist air (Garreaud *et al*., 2008). Another low level jet in South America exists along the subtropical west coast. It is driven by the high pressure cell in the SE-Pacific and transports air masses from south to north (Garreaud, 2005).

Dry regions

South America contains three major dry regions, which are (*i*) the Peru-Chile coastal desert, (*ii*) NE-Brazil and (*iii*) SE-Argentina. The first is caused by subsiding air of the high pressure cell in the SE-Pacific. In addition, the cold Humboldt Current causes a thermal inversion with cold air at sea level and warm air higher up, leading to fog and stratus clouds, but not to rain. The dryness in NE-Brazil is the consequence of subsiding air driven by convection over the Amazon

basin (Hewitt and Jackson, 2003) or over the Atlantic Ocean (Garreaud *et al.,* 2008). The Dryness in SE-Argentina is mainly due to the lee-effect of the Andes.

El Niño

The El Niño/Southern Oscillation (ENSO) is the major source of interannual variability over much of South America. In most years, when El Niño is not occurring, easterly trade winds push the warm surface waters of the Pacific westward, leading to a deeper warm layer water in the west, compared to the east Pacific. The warm surface waters in the west are associated with a low pressure cell, promoting convection and rainfall in Indonesia. The cold waters in the east Pacific are associated with a high pressure cell and thus low precipitation. El Niño describes events, where the mentioned pressure cells and easterly trade winds weaken, causing the warm surface waters in the Pacific to move eastwards, impeding the upwelling of cold surface water in coastal Ecuador and Peru. Among the impacts are (*i*) decrease of precipitation over northern South America, (*ii*) increase of precipitation in south-eastern South America (*iii*) flood conditions in southern Ecuador and northern Peru (*iv*) less snow accumulation in Andean glaciers and (*v*) drought in NE Brazil. With respect to Bolivia, El Niño is associated with rainfall deficit in the Altiplano, Andean mountain ranges, inter-Andean valleys and the Chaco region and excess of rainfall in the north-eastern plains (Ibisch and Merida, 2003). Recent ENSO events occurred during 2006/07, 2004/05, 2002/03, 1997/98, 1993/94, 1991/92 and 1986/87.

2 Methodology

2.1 Experimental design

The regional climate model (RCM) PRECIS (Providing Regional Climates for Impact Studies, Jones *et al.,* 2004) is implemented for Bolivia for the slots 1961-1990, 2001-2030 and 2071-2100. Simulations are run for three different emission scenarios (SRES, Table 9) and four different lateral boundary conditions (LBC, chapter 2.5.1). PRECIS is run for two spatial resolutions, which are 0.44 degree and 0.22 degree, which correspond approximately to 50km and 25km respectively. Table 1 summarizes the experimental design.

Table 1 Experimental design

	1961-1990	2001-2030			2071-2100		
LBC	baseline	A2	B2	A1B	A2	B2	A1B
ECHAM4	x	x	x	-	x	x	-
HadAM3P	x	-	-	-	x	x	-
HadCM3Q	x	-	-	x	-	-	x
ERA40	x	-	-	-	-	-	-

2.2 Validation design

The validation consists of four separate comparisons where (a) the GCM is compared to observations, (b) three RCM are compared to observations, (c) ERA40 (see chapter 2.5.1) is compared to observations and (c) the most realistic RCM is compared to its corresponding GCM. The comparison corresponds to the slot 1961-1990. The author compares 30 year seasonal climatic variables including temperature and precipitation with respect to their mean, root mean square error (RMS, see Eq. 1) and spatial correlation (*r*). The author applies the *t*-test (Eq. 2) in order to determine whether two data sets are significantly different from one another or not. Differences between simulation and observation are inevitable. They may be due to three potential sources of errors, which are observational data, lateral boundary conditions (LBC, see 2.5.1) and/or internal physics of PRECIS. In order to have full transparency about the quality of the observational data, the author does not use global surface climatology such as CRU (New *et al*., 1999), but conducts his own spatial interpolation of meteorological measurements using different interpolation techniques such as kriging. The quality of the derived climatology is assessed by general cross validation (New *et al.,* 1999). To eradicate the error introduced by the

spatial interpolation, the author additionally compares modeled and observed data only at the locations of the meteorological stations. Further, whether differences between observation and simulation are due to PRECIS or LBC is assessed by running PRECIS with ERA40. ERA40 presents quasi-observational data and fulfills the explicit purpose of error analysis. If the PRECIS ERA40 run shows the same error as the PRECIS run of concern, then the error is not due to the LBC applied but due to internal physics of PRECIS. On contrary, when the error disappears, the error is due to the LBC applied (Taylor *et al.,* 2001). Table 2 summarizes the design of the proposed validation. The RMS is obtained according to Stull (2000),

$$RMS = \sqrt{\frac{\sum_{i=1}^{N}(a_i - b_i)^2}{N}}, \quad \text{(Eq. 1)}$$

where *a* is the modeled and *b* the observed variable.

The two-sided *t*-test for the comparison of two means of independent samples is obtained according to Köhler *et al.,* (2002),

$$s_D = \sqrt{\frac{(n_1-1)s_x^2+(n_2-1)s_y^2}{n_1+n_2-2}}, \quad \text{(Eq. 2)}$$

$$t_{Vers} = \frac{|\bar{x}-\bar{y}|}{s_D} \cdot \sqrt{\frac{n}{2}}, \quad \text{(Eq. 3)}$$

where n_i is the sample size and s_x^2 and s_y^2 are the variances of the observed (x) and the modeled (y) meteorological variable. Is $t_{Vers} \leq t_{Tab}$, then both data sets are not significantly different from another. t_{Tab} is obtained from a *t*-table; an α of 0.05 is chosen.

Table 2 Validation design

ID	Compare	with	time slot	Objective
a	GCM	observation	1961-1990	Performance of the GCM
b	RCM LBC	observation	1961-1990	Performance of the RCM
c	RCM ERA	observation	1961-1990	Error analysis
d	RCM LBC	GCM	1961-1990	Consistency between RCM and GCM

2.3 Study area

The RCM is applied to the rectangular boundaries of Bolivia, covering about 2,651,740 km^2 (1,612km x 1,640km) of heterogeneous terrain. Bolivia covers 10% of the tropical forests of South America and is among the 15 most biodivers countries of the world (Molina *et al*., 2009). Its territory measures more than one million square kilometers (twice the size of Spain) with altitudes ranging from 70 to 6,500 m.a.s.l. (Figure 7). Bolivia contains 12 contrastig ecoregions including rainforests, cloud forests, dry forests, grasslands, wetlands and highland vegetation (Ibisch and Mérida, 2003). Bolivia's topography ranges from 70 to 6,500 m.s.l. and from Amazonian rainforest to highland desserts (Figure 7). Species distribution is constrained by an altitudinal gradient of the eastern slope of the Andes and by a latitudinal gradient with increasing precipitation towards the north (Killeen *et al.,* 2008). The analysis reduces this extreme diversity by dividing the country into its three major regions, which are (*a*) the lowlands (<800m.s.l.), (*b*) the sub-Andean mountain range (800-3,200 m.s.l.) and (*c*) the highlands (>3,200m.s.l.) (Ibisch and Mérida, 2003) (Figure 8).

2.4 Model description

PRECIS consists of a coupled atmospheric and land surface model describing processes related to dynamical flow, atmospheric sulfur cycle, clouds, precipitation, radiation, land surface and deep soil. The atmospheric model is based on the atmospheric component of the GCM HadCM3 (Gordon *et al.,* 2000), whereas the land surface model is taken from MOSES (Met Office Surface Exchange Scheme, Cox *et al.,* 1999). To run, PRECIS demands prognostic variables

which provide information about atmospheric dynamics at the edges of the model domain. The prognostic variables consist of surface pressure, winds, temperature and moisture. Additionally, five chemical species are used to simulate the spatial distribution of sulphate aerosols. Applying parameterization, PRECIS uses the prognostic variables to derive diagnostic variables. The latter consist of information on clouds, precipitation, atmospheric aerosols, boundary layer processes, land surface processes and gravity wave drag. The prognostic variables are obtained from GCM and form the Lateral Boundary Conditions (LBC) of the model domain. Precipitation is modeled as large scale movement of air masses and as a result of convection. Cloud formation is calculated from simulated atmospheric profiles of temperature, pressure, humidity and aerosol concentration. The conversion of cloud water to precipitation depends on the amount of cloud water present and precipitation falling into the grid box from above, causing a seeder-feeder enhancement. A full description of the model and its parameterization scheme is documented in Jones *et al.,* (2004).

2.5 Data

2.5.1 Lateral Boundary Conditions

The input data consists of the Lateral Boundary Conditions (LBC) of the model domain. This research uses 3 LBC from the GCM ECHAM4 (Roeckner *et al.,* 1996), HadAM3P, HadCM3Q (Gordon *et al.,* 2000), and the observational re-analysis data ERA40 (Uppala *et al.,* 2005). The first GCM is generated by the Max Planck Institute in Germany and the latter by the Met Office Hadley Centre in Great Britain. ERA40 is a re-analysis of meteorological observations from September 1957 to August 2002 and is produced by the European Centre for Medium-Range Weather Forecasts (ECMWF). ERA40 is an input, but is used for validation purposes.

2.5.2 Meteorological observations

The meteorological observations used for validation purposes are obtained from Bolivia's National Service of Meteorology and Hydrology (SENAMHI). The observations present 30 year monthly means valid for the period 1961-1990. The data includes absolute air temperature at 1.5m above the surface measured from 54 and monthly accumulated precipitation measured from 57 meteorological stations (Figure 8).

2.5.3 Spatial interpolation of meteorological observations

Meteorological observations are spatially interpolated applying geo-statistical models. This implies (a) exploring the data with respect to correlations, distribution and spatial trends, (b) fitting different interpolation models, (c) validating the different models using cross-validation and (c) comparing the statistical performance of the models.

Air temperature

A local lapse rate (Γ) is calculated by expressing the annul 30 year mean air temperature as a linear function of surface elevation (Figure 14). With an $R^2 = 0.968$, Γ is estimated to be 4K/km, which is lower than the standard atmospheric lapse rate of 6.5K/km (Stull, 2000). Next, mean absolute air temperature measurements are converted to potential air temperature (θ), applying Γ in Equation 4. After spatially interpolating θ, the values are converted back to actual air temperature values applying Γ and a digital elevation model (DEM) (Eq. 5). According to Stull (2000),

$$\theta = T + \Gamma * z \,, \qquad \text{(Eq. 4)}$$

$$T(x,y) = \theta(x,y) - \Gamma * z \,, \qquad \text{(Eq. 5)}$$

where T is absolute air temperature (K) measured at meteorological station, θ is potential air temperature (K), Γ is local lapse rate (Γ = 0.4 K/km), z is surface elevation (m), $\theta\ (x,y)$ is spatially interpolated potential air temperature (K) and $T(x,y)$ is absolute air temperature for

every pixel (K). The interpolation error reduces when the data is normally distributed. The histogram in Figure 15 reveals that the data is not normally distributed but is negatively skewed with a coefficient of skewness equal to -0.65. However, the data is still considered to be good enough for interpolation since the distribution contains only one peak and the skewness is moderate. The data must also be analyzed with respect to any potential trends. If the data does contain a trend it must be removed before and again added after the interpolation. The trend analysis visualized in Figure 16 shows a quadratic trend in the north-east direction (2^{nd} order polynomial, blue graph) and no trend in the north-west (red graph) or any other direction. There are unlimited options to fit models for spatial interpolation. Here, 4 different models are tested with annual mean temperature data (Table 10). Model 1-3 are based on kriging of θ. Model 1 does not include a trend removal and model 3 includes anisotropy, i.e. directional influence. Model 4 is based on co-kriging of actual air temperature (T) with elevation being the co-variable. Comparing RMS and mean standard error of every model shows that the models can be ranked as follows: m3, m2, m1 and m4, where the first is the most superior model. Despite its low error, model 4 is rejected because it produces a very artificial surface with trends which cannot be explained by the author. Thus, model 1 and model 2 are examined in more depth on a monthly basis (Table 11). With respect to RMS, in half of the cases model 2 and in the other half model 1 is superior. With respect to the mean standard error however, model 2 is superior over model 1 in all 12 months. Thus, model 2 with an RMS of 0.94°C is chosen for the spatial interpolation of θ. An example of a actual temperature map is given in Figure 9. To compare observational data with the model results from PRECIS, the interpolated data is aggregated to a spatial resolution of 0.44 and 0.22 decimal degrees. Both datasets cover the exact same extent and the pixels are shifted such that all pixel borders are consistent.

Precipitation

The precipitation data is analyzed with respect to a possible correlation with surface altitude, its distribution and trends. Figure 14 plots annual precipitation against surface altitude. Both variables are correlated and a potential function with an $R^2 = 0.762$ can be fitted to the data. However, there are 3 outliers between 1000-2000m where observed precipitation is much higher than the fitted function. The 3 outliers are the stations Apolo, Chulumani and Irupana, all located in the department of La Paz and within or at the margin of an ecoregion characterized as cloud forest. It is likely that a more complete coverage of meteorological stations would reveal a more complex relationship between precipitation and altitude. Thus, the interpolation technique should take altitude into account, but should not be a deterministic approach. The histogram in Figure 15 shows that the data is positively skewed and not normally distributed. The trend analysis in Figure 16 shows a linear increase in the NE-direction and second order polynomial trend in the SE-direction. The spatial analysis shows the complexity of the data and indicates that a high error can be expected when interpolating the results spatially. 9 interpolation models are tested and statistically compared in Table 10. The models include kriging and co-kriging with altitude and a trend removal of first and second order. The model with the lowest RMS is the simplest one (model 1, kriging, no trend removal). To include the orographic effect on precipitation though, model 6 with a slightly higher RMS of 15.52 mm/month is chosen. The RMS of 15.52 mm/month presents 20% of the mean observed precipitation and is therefore, as expected very high. Applying model 6 to monthly precipitation data, the RMS even increases to 38% (Table 12).

2.5.4 Data extraction

The PRECIS output files of interest are monthly *.pp*-files. The author runs a shell-script which calculates 30-year mean monthly grids, removes a buffer edge around the model domain, re-grids the files, converts the data to the desired physical unit and converts the data format into text-files. The spin-up year is excluded from this process. The text-files are converted to grid-files in the GIS-software ArcGIS and split up into four regions, which are Bolivia, lowlands, sub-Andes and highlands. For the statistical analysis, the data is exported to excel.

3 Results

The results consist of high resolution daily information on processes related to dynamical flow, atmospheric sulfur cycle, clouds, precipitation, radiation, land surface and deep soil. Here, only 30-year monthly mean values from 1961-1990 of temperature and precipitation are analyzed and compared to meteorological observations. Figure 9 shows air temperature and precipitation for the GCM-ECHAM4, RCM-ECHAM4 and observations.

3.1 Historic climate (1961-1990)

3.1.1 Grid-to-grid analysis

Air temperature

Figure 1 compares mean air temperature of the four models with spatially interpolated observations on a monthly basis. The observations show a seasonal temperature cycle with highest values from Dec-Jan and lowest values from Jun-Jul for all three regions. All models follow this seasonal cycle. The models underestimate the observed temperature in all 12 months in case of sub-Andes and highlands and in 9 months in case of the lowlands. The monthly RMS of the models is given in Figure 17 for each region explicitly. The models behave similar in the highlands and contrary in lowlands and sub-Andes. Generally, RMS-values are lowest in the lowlands (1.5°C), medium in the Sub-Andes (2.8°C) and highest in the highlands (3.2°C) (Table 3). The spatial correlation between models and observation is very high (0.977-0.989) and constant throughout the year when looking at Bolivia as a whole. When looking at the three sub-regions respectively though, *r* decreases and differences among models become more visible (Figure 17). The change of *r* throughout the year is similar among models but different for each region. *r* is lowest in the lowlands (0.71), medium in the highlands (0.81) and highest in the sub-Andes (0.85) (Table 3). When comparing the annual mean RMS and *r* of the 4 models, ECHAM4 results to have the smallest RMS in all regions and HadCM3Q has the highest *r* in all regions (Table 3).

Table 3 Annual mean RMS and spatial correlation of mean air temperature

Region	Temperature	ECHAM4	HadAM3P	HadCM3Q	ERA40	model mean	best model
Lowlands	RMS[1]	1.27	1.54	1.82	1.35	1.5	ECHAM4
	r[1]	0.723	0.697	0.727	0.71	0.714	HadCM3Q
	model = obs[2]	1	2	1	1	1.25	HadAM3P
Sub-Andes	RMS[1]	2.58	3.02	3.09	2.68	2.84	ECHAM4
	r[1]	0.856	0.852	0.858	0.849	0.854	HadCM3Q
	model = obs[2]	3	0	0	1	1	ECHAM4
Highlands	RMS[1]	2.69	3.54	3.67	2.85	3.19	ECHAM4
	r[1]	0.801	0.794	0.826	0.804	0.807	HadCM3Q
	model = obs[2]	2	0	0	2	1	ECH., ERA40
Bolivia	RMS[1]	1.93	3.58	2.55	2	2.52	ECHAM4
	r[1]	0.983	0.982	0.984	0.983	0.983	HadCM3Q
	model = obs[2]	5	2	2	4	3.25	ECHAM4

[1] annual mean, [2] # months where there is no significant difference between model and observation (*t*-test, $\alpha = 0.05$)

Precipitation

Figure 1 compares modeled and observed precipitation on a monthly basis. The observations show a seasonal precipitation cycle with highest values from Dec-Jan and lowest values from Jun-Jul for all three regions. All models follow this seasonal cycle. All models overestimate precipitation significantly for all months in the sub-Andean mountain range and almost all months in the highlands. In the lowlands, over and underestimation are balanced. The RMS

expressed as percentage of monthly mean observed precipitation is lower in the lowlands (61% of the observed amount), higher in the sub-Andean mountain range (284%) and highest in the highlands (355%) (Table 4). The spatial correlation between modeled and observed precipitation is highest in the highlands and lowest in the lowlands.

Table 4 Annual mean RMS- error and spatial correlation of monthly precipitation

Region	Precipitation	ECHAM4	HadAM3P	HadCM3Q	ERA40	model mean	best model
Lowlands	RMS (%)[1]	54	57	66	68	61	ECHAM4
	r[1]	0.36	0.32	0.17	0.16	0.25	ECHAM4
	model = obs[2]	0	2	1	0	0.75	HadAM3P
Sub-Andes	RMS (%)[1]	212	270	270	384	284	ECHAM4
	r[1]	0.62	0.62	0.61	0.59	0.61	ECHAM4
	model = obs[2]	0	0	0	0	0	-
Highlands	RMS (%)[1]	254	338	327	502	355	ECHAM4
	r[1]	0.69	0.7	0.68	0.71	0.7	ERA., HadAM3P
	model = obs[2]	1	1	0	0	0.5	ECH., HadAM3P
Bolivia	RMS (%)[1]	91	547	113	144	224	ECHAM4
	r[1]	0.45	0.37	0.3	0.3	0.35	ECHAM4
	model = obs[2]	1	1	2	0	1	HadCM3Q

[1] annual mean, [2] # months where there is no significant difference between model and observation (t-test, $\alpha = 0.05$)

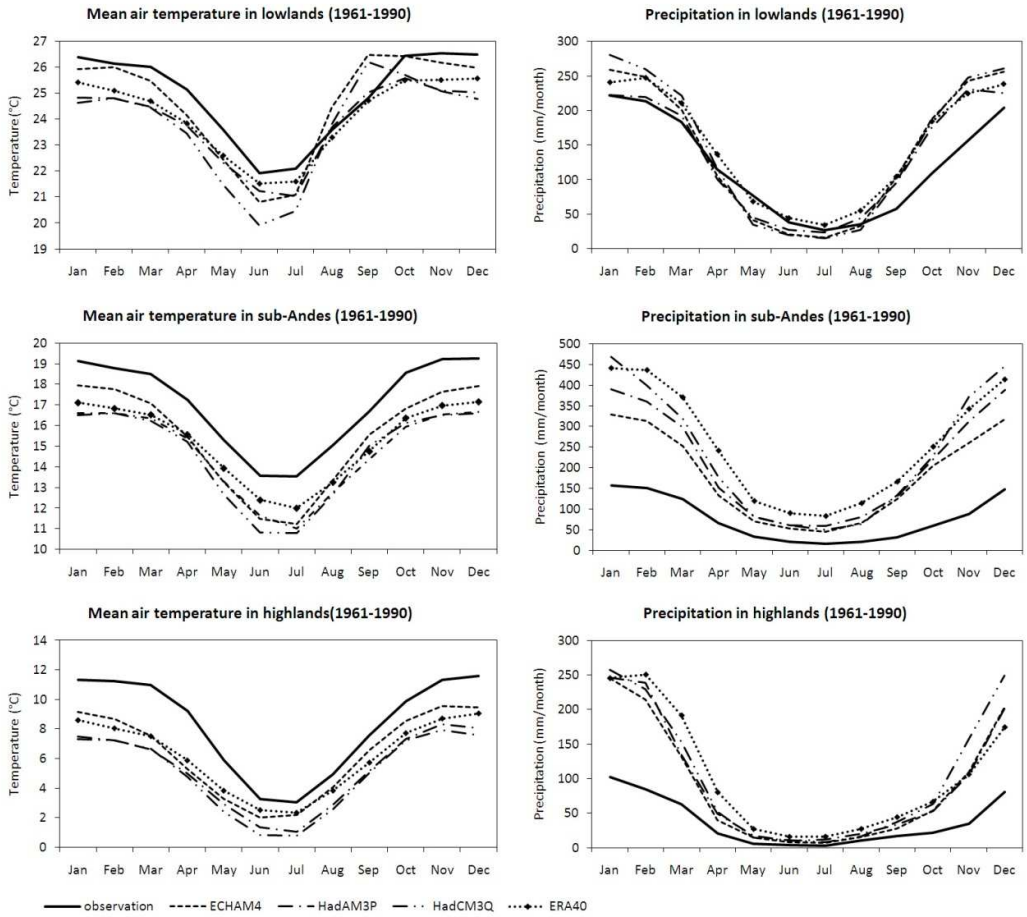

Figure 1 Modeled and observed seasonal temperature (left) and precipitation cycle (right). The models include the PRECIS runs with ECHAM4, HadAM3P, HadCM3Q and ERA40.

3.1.2 Comparing GCM, RCM and observations

Figure 2 compares the GCM ECHAM4, RCM ECHAM4 (50km) and RCM ECHAM4 (25km) with observed temperature and precipitation. With respect to temperature, the RCM-data is more similar to observations than the GCM-data and the 25km-resolution data is closer to the observations than the 50-km data. With respect to precipitation it is the other way around. Here, the GCM-data is much more similar to observations than the RCM-data and the 50km resolution is a bit closer to observations than the 25-km data. The similarity between precipitation modeled by the GCM and observations in the highlands is striking.

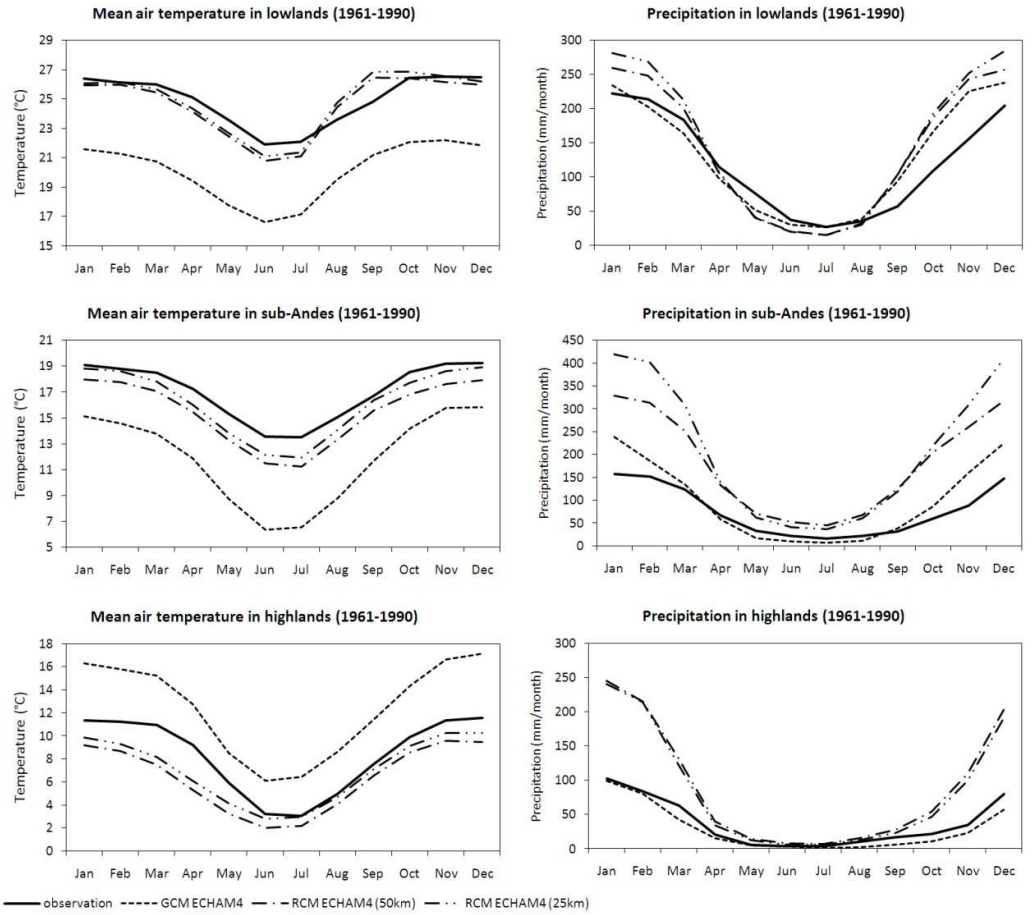

Figure 2 Modeled and observed seasonal temperature (left) and precipitation cycle (right). The models include the GCM ECHAM4, and the PRECIS runs with ECHAM4 of 50km and 25km spatial resolution.

3.1.3 Point-to-point analysis

The spatial interpolation of observed data introduces an additional error source. To eradicate this error, PRECIS results from ECHAM4 with a spatial resolution 0.22 degrees (approximately 25km) are compared to meteorological observations, GCM and ERA40 at the location of the meteorological stations (Table 13).

Air temperature

The countrywide RMS of temperature is estimated to be 3.8°C with 1.4°C, 4.9°C and 5.5°C in lowlands, sub-Andes and highlands respectively. Figure 3 shows that the model systematically underestimates temperature in the sub-Andes and the highlands. In the low-lands no systematic error exists. The country-wide spatial correlation is 0.91 (-), with lower values in the highlands.

According to the *t*-test, modeled and observed temperature are significantly different in the sub-Andes and highlands and not significantly different in the lowlands.

Precipitation

The countrywide RMS of precipitation is estimated to be 119 mm/month, which corresponds to 150% of the average observed precipitation. The RMS is lower in the lowlands (62%) and higher in the sub-Andes and highlands (256% and 252%). The model systematically overestimates precipitation in the sub-Andes and highlands (Figure 3). The country-wide spatial correlation is 0.73 (-). According to the *t*-test, modeled and observed monthly precipitation are significantly different in all regions.

Table 5 Summary of the result of the *t*-test ($\alpha = 0.05$)

Is *y* significantly different from *x*?			Temperature			Precipitation		
y	*x*	time slot	Lowlands	Sub-Andes	Highlands	Lowlands	Sub-Andes	Highlands
GCM	OBS	1961-1990	yes	yes	yes	**no**	**no**	yes
RCM LBC	OBS	1961-1990	**no**	yes	yes	yes	yes	yes
RCM ERA	OBS	1961-1990	yes	yes	yes	yes	yes	yes
RCM LBC	GCM	1961-1990	yes	yes	yes	yes	yes	yes

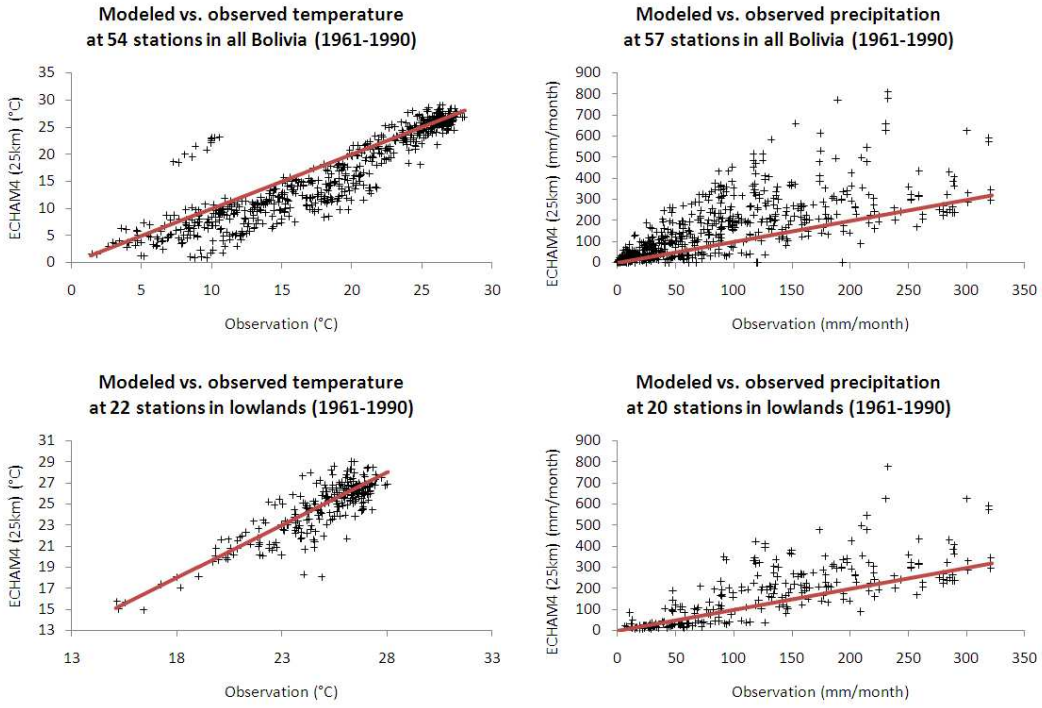

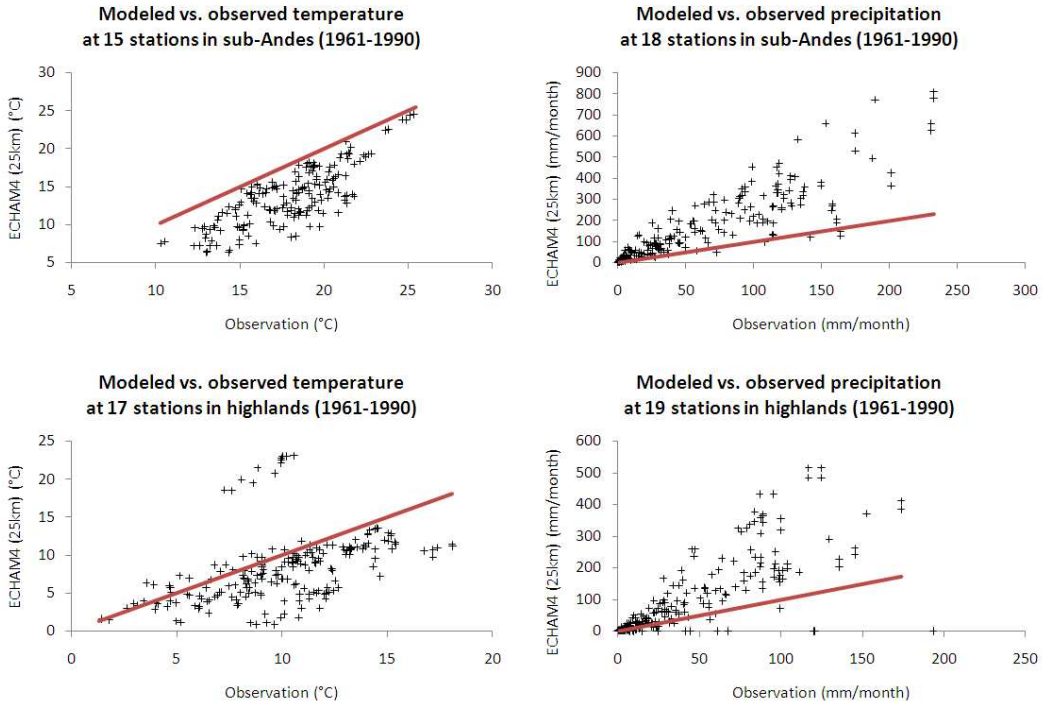

Figure 3 Modeled versus observed temperature (left) and precipitation (right) at the location of meteorological stations. The red line shows where the model equals the observation.

3.2 Climate Change

3.2.1 Observed tendencies

To the knowledge of the author, only a single unpublished report examines historic changes in temperature and precipitation in Bolivia from meteorological observations (Ontiverus). The analysis is based on daily temperature and precipitation extremes from 1941-2004 from 19 stations. The main conclusions are that (*i*) daily minimum air temperature is significantly increasing and that this increase is most pronounced in the extreme north and south of the country. With respect to precipitation, Ontiverus concludes (*ii*) more humid conditions in the northern and central part of the lowlands and in the central parts of the sub-Andes. Furthermore (*iii*) increasing drier conditions are observed in the highlands and the southern tip of the lowlands.

3.2.2 Modeled tendencies

Climate change is analyzed with respect to the PRECIS results from the ECHAM4-run with a spatial resolution of 25km. Changes of temperature and precipitation are summarized in Table 6 and Table 7 respectively. The numbers given in the text of this chapter present the means of the SRES A2 and B2.

Air temperature

Temperature increases in all Bolivia under both SRES with highest temperatures for the SRES A2 (Figure 4). By 2030, temperature increases by about 1.3°C, 1.2°C and 1.4°C in lowlands, sub-Andes and highlands respectively. By 2100 temperature increases by about 4.7°C, 4.2°C and 5.2°C in lowlands, sub-Andes and highlands respectively. In most cases, the strongest temperature increase happens around August. The annual mean temperature increase by 2030 and 2100 is shown in Figure 6. The figure reveals that the highlands and the northern part of Bolivia, which cover highland vegetation and Amazon forest respectively, experience the strongest increase of temperature. This tendency is confirmed by meteorological observations

(see chapter 3.2.1). The lowlands show a latitudinal temperature gradient with an increasing change of temperature in the north direction. This tendency becomes even more pronounced in 2100. Monthly temperature change maps for SRES A2 are given in Figure 10 (2001-2030) and Figure 12 (2071-2100).

Changes in climate variability are quantified by comparing the standard deviations of the spatial and temporal information on air temperature. The changes of the standard deviations are less than 1°C. Generally, spatial variability slightly increases in the lowlands and stays about the same or slightly decreases in the sub-Andes and highlands. Temporal variability slightly increases in lowlands and sub-Andes and shows contradictory results in the highlands.

Precipitation

The precipitation cycle intensifies, with more precipitation during the rain- and less precipitation during the dry season. This intensification is more pronounced in case of the SRES A2 compared to B2. Most maximum relative increases of precipitation occur from April to June and most maximum relative decreases of precipitation occur from July to August. The following numbers present the means of A2 and B2 results as given in Table 6 and Table 7. By 2030, precipitation decreases maximum by about -28%, -11% and -19% in lowlands, sub-Andes and highlands respectively. During the same slot, precipitation increases maximum by about 17%, 8% and 25% in lowlands, sub-Andes and highlands respectively. By 2100, precipitation decreases maximum by about -36%, -15% and -32% in lowlands, sub-Andes and highlands respectively. During the same slot, precipitation increases maximum by about 45%, 38% and 36% in lowlands, sub-Andes and highlands respectively. Figure 6 shows the net change of yearly precipitation (center) and the number of months where mean monthly precipitation is greater by 2030 and 2100 than in 1990 (right). Most of the annual net precipitation decrease occurs in the highlands and to some extent in the northern part of the lowlands (Amazon forest). Most of the annual net increase of precipitation occurs in the southern part of the lowlands (dry forests) and to some extent in the northern part of the sub-Andes. The distribution of wetter and drier months follows this pattern. Observed tendencies as presented in chapter 3.2.1 confirm modeled tendencies only with respect to drier conditions in the highlands. A drying in the northern part of Bolivia is not observed yet. Monthly maps of precipitation change are given in Figure 11 for 2001-2030 and in Figure 13 for 2071-2100 (ECHAM4, SRES A2).

In contrary to temperature, the variability of precipitation is not quantified through the standard deviation but through the coefficient of variance (*cv*), which is equal to the standard deviation divided by the absolute sample mean. By 2030, the spatial variability of precipitation increases by about 3%, 2% and 13% in lowlands, sub-Andes and highlands. The temporal variability stays about the same till 2030. By 2100, the spatial variability of precipitation increases by about 5%, 6% and 41% and the temporal variability changes by about 4%, -1% and 5% in lowlands, sub-Andes and highlands.

Table 6 Change of air temperature mean, spatial- and temporal standard deviation of the ECHAM4-run (25km) in lowlands, sub-Andes and highlands in 2001-2030 and 2071-2100 for the SRES A2 and B2.

Temperature	ECHAM4 (25km)	2001-2030		2071-2100	
Region	Variable	A2	B2	A2	B2
Lowlands	ΔT_{mean} (ºC)	1.34	1.17	5.49	3.92
	month of ΔT_{max}	AUG	AUG	SEP	AUG
	Δ spatial std dev	0.1	0.08	0.59	0.39
	Δ temporal std dev	0.05	0.12	0.17	0.04
Sub-Andes	ΔT_{mean} (ºC)	1.25	1.08	4.84	3.51
	month of ΔT_{max}	AUG	DEC	SEP	JUL
	Δ spatial std dev	-0.06	-0.04	-0.16	-0.15
	Δ temoral std dev	0.03	0.11	-0.11	-0.06
Highlands	ΔT_{mean} (ºC)	1.57	1.27	5.96	4.44
	month of ΔT_{max}	NOV	DEC	JUL	JUL
	Δ spatial std dev	-0.04	0	-0.06	-0.04
	Δ temporal std dev	0.11	0.2	-0.13	-0.11

Table 7 Change of precipitation mean, spatial- and temporal variation coefficient of the ECHAM4-run (25km) in lowlands, sub-Andes and highlands in 2001-2030 and 2071-2100 for the SRES A2 and B2.

Precipitation	ECHAM4 (25km)	2001-2030		2071-2100	
Region	Variable	A2	B2	A2	B2
Lowlands	max. neg. Δ*P*(%)	-38.72	-16.81	-36.01	-35.78
	max. pos. Δ*P*(%)	16.26	18.44	52.97	37.21
	month max. neg. Δ*P*(%)	JUL	JUL	SEP	AUG
	month max. pos. Δ*P*(%)	APR	MAY	APR	APR
	Δ spatial *cv* (%)	7.8	-2.25	2.64	7.16
	Δ temporal *cv* (%)	1.26	0.67	4.56	4.42
Sub-Andes	max. neg. Δ*P*(%)	-8.14	-14.12	-11.66	-18.29
	max. pos. Δ*P*(%)	10.66	5.51	50.3	26.03
	month max. neg. Δ*P*(%)	JUL	AUG	AUG	AUG
	month max. pos. Δ*P*(%)	APR	NOV	JUN	JUN
	Δ spatial *cv* (%)	3.1	1.72	4.99	6.92
	Δ temporal *cv* (%)	-0.64	0.1	-2.77	-0.16
Highlands	max. neg. Δ*P*(%)	-26.39	-11.67	-37.22	-26.48
	max. pos. Δ*P*(%)	26.43	22.97	49.46	21.55
	month max. neg. Δ*P*(%)	MAY	JUN	DEC	NOV
	month max. pos. Δ*P*(%)	APR	APR	JUL	SEP
	Δ spatial *cv* (%)	17.77	7.64	38.16	44.34
	Δ temporal *cv* (%)	-0.01	-2.43	3.61	7.18

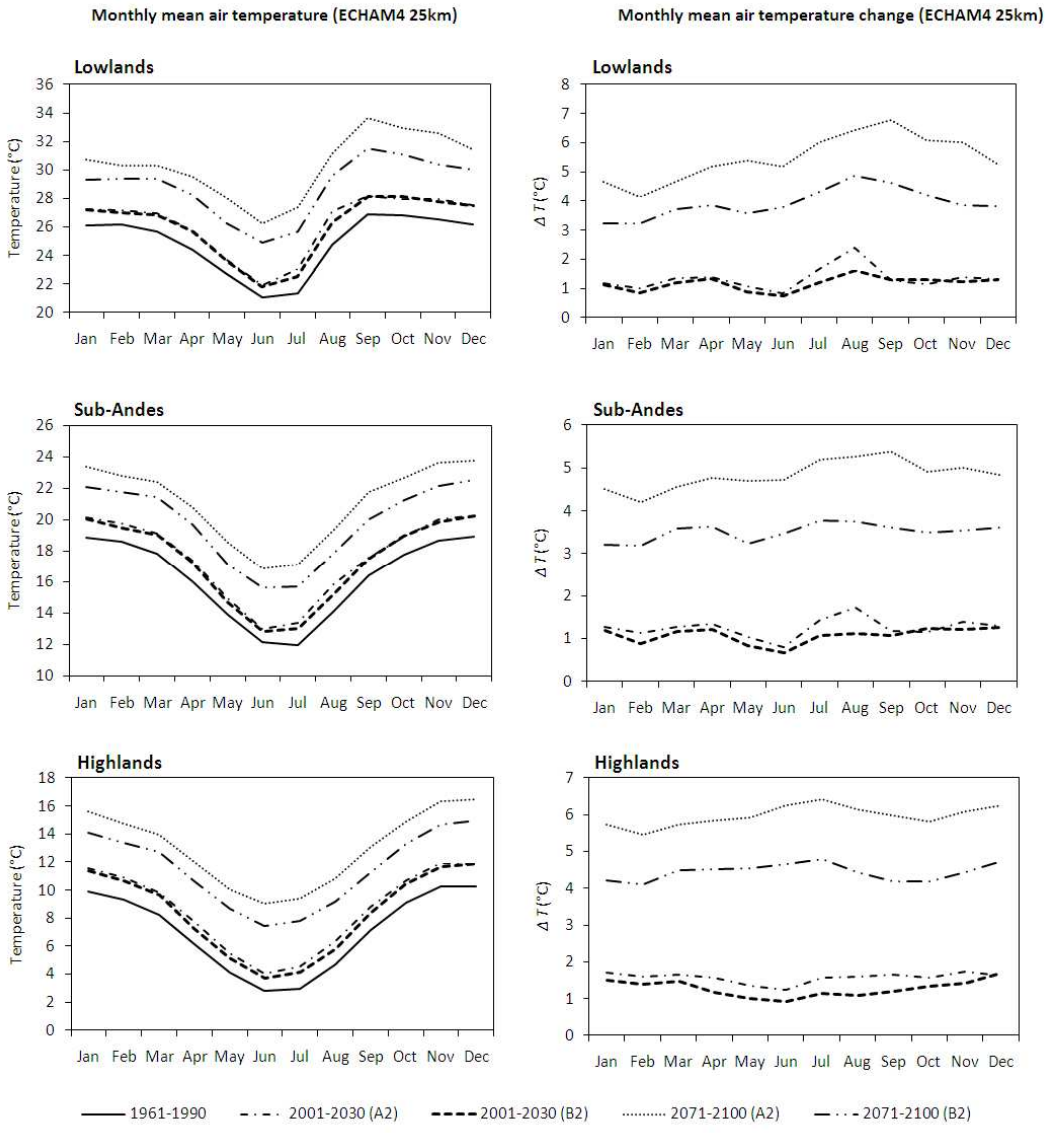

Figure 4 Monthly mean air temperature (left) and monthly mean air temperature change (right) of the ECHAM4-run (25km) in lowlands, sub-Andes and highlands in 1961-1990, 2001-2030 and 2071-2100 for the SRES A2 and B2.

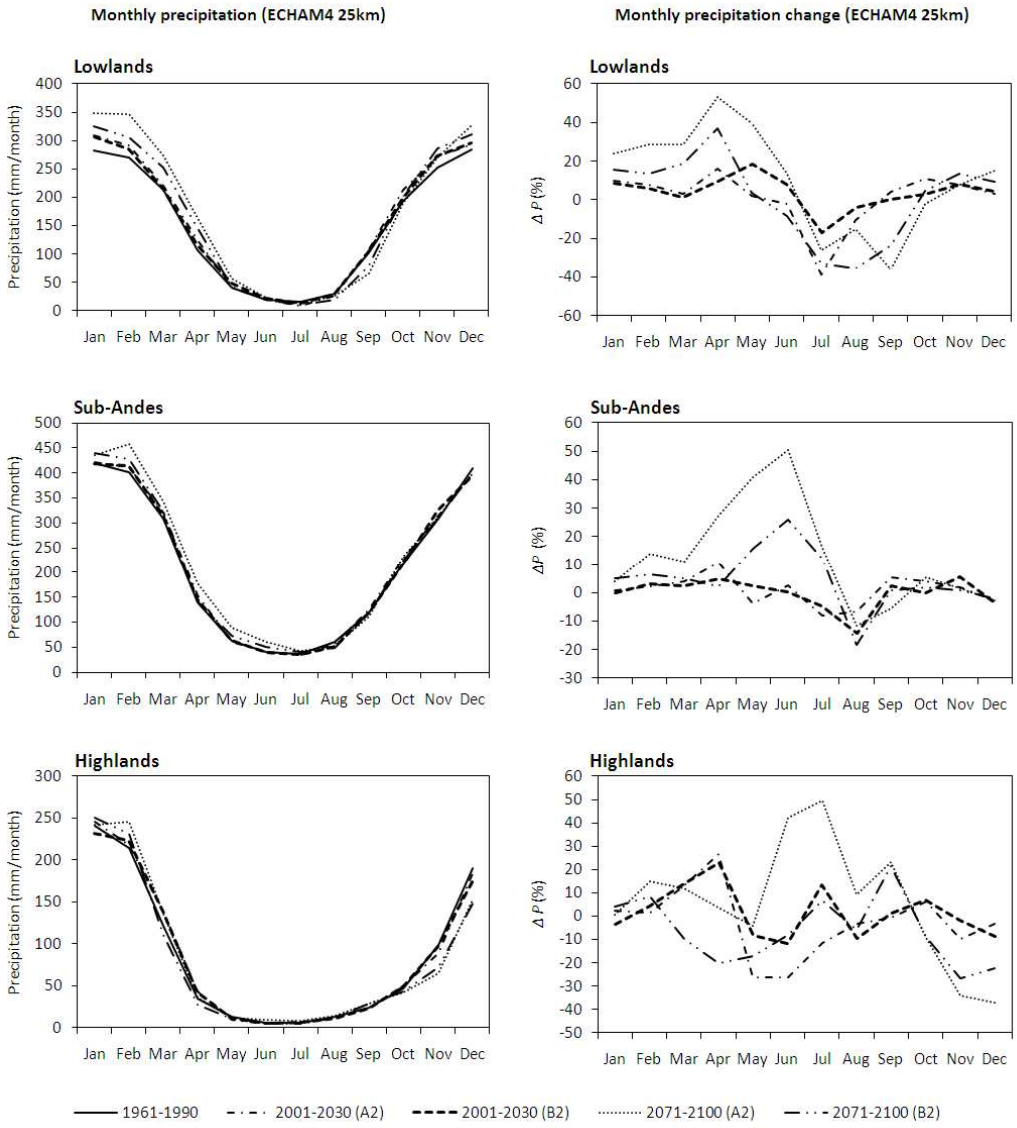

Figure 5 Monthly mean precipitation (left) and monthly mean precipitation change (right) of the ECHAM4-run (25km) in lowlands, sub-Andes and highlands in 1961-1990, 2001-2030 and 2071-2100 for the SRES A2 and B2.

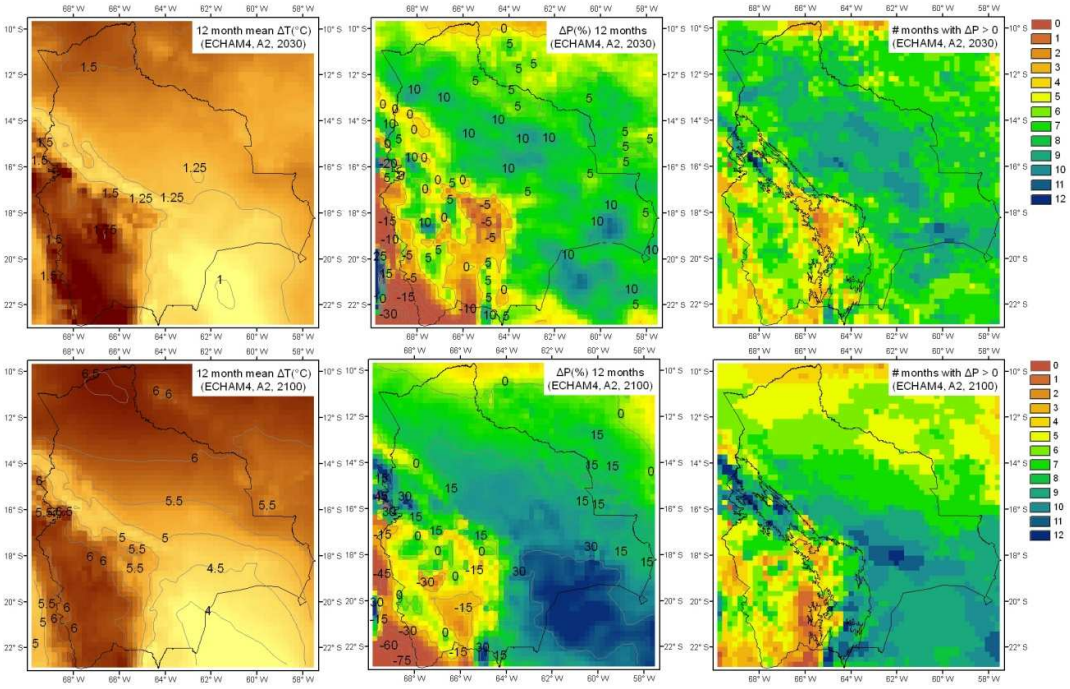

Figure 6 Annual mean change of air temperature (left) and precipitation (center) and numbers of months with an increase of monthly mean precipitation (right) for 2001-2030 (above) and 2071-2100 (below) (ECHAM4, A2)

4 Error analysis

4.1 Observational data

The quality of the observational data depends e.g. on (*i*) the quality of the measurement instruments, (*ii*) the completeness of the time series, (*iii*) the representativeness of the spatial coverage of the stations and (*iv*) the quality of the spatial interpolation. Since the bias is systematic, (*i*) and (*ii*) are unlikely the main error source. (*iii*) is likely to play a role, since in the highlands, stations are located only at the eastern margins of the region and in the sub-Andean mountain range, spatial variability due to orographic effects are expected to be extremely high. However, since the error is clearly systematic, the low density of stations is not considered to be the major error source. (*iv*) is not the main error source, since two- and one-dimensional comparisons lead to the same tendencies. Thus, the quality of the observational data is not considered to be the main error source.

4.2 Lateral Boundary Conditions

LBC present the main error source if the PRECIS results obtained from ERA-40 are substantially better than the PRECIS results obtained from other LBC data. Since this is not the case, and since the GCM ECHAM4 shows temperature values closer to observations than RCM-results, the LBC is unlikely to be the major error source.

4.3 PRECIS

Since observational data and lateral boundary conditions do not appear to be the main error source, PRECIS itself is likely to be the reason for the underestimation of temperature and overestimation of precipitation in highlands and Sub-Andes. This conclusion is confirmed by the findings, that several RCM applications show a bigger bias in high- than lowlands (see chapter 1.2). The failure may be related to an inaccurate representation of the topography and/or to the parameterization schemes. It is beyond the scope of this evaluation to examine the applicability of PRECIS' parameterizations for the Bolivian climatology. Instead, the bias for Bolivia is compared to the bias of other RCM-applications to evaluate, whether the error is

within a typical range. Table 14 lists the bias of 31 RCM applications in Europe, Asia, Africa and South America. With respect to air temperature, the 31 RCM show a mean bias of 1.65°C with a standard deviation of 0.95°C. With respect to precipitation, the bias is 21% with a standard deviation of 9%. Applying this range, the PRECIS application in Bolivia lies within an acceptable error-range only with respect to temperature in the lowlands. The comparison has limited validity, because this study quantifies the difference between modeled and observed data by RMS, while the RMC applications express differences as bias. RMS and bias are equal if the error is systematic; RMS is bigger than the bias if the error is arbitrary.

5 Conclusions and discussion

Recent climate

- GCM, RCM and observations show a seasonal temperature and precipitation cycle. The months of modeled and observed minimum and maximum values, match.
- Modeled and observed data are correlated.
- The LBC ECHAM4 leads to lower RMS compared to the other LBC.
- Due to the low density of the meteorological stations and the heterogeneity of Bolivia's topography, the quality of the spatially interpolated observational data is limited, however, it is not considered to be the main error source.
- The error analysis indicates that the cold and wet bias is unlikely due to observations or LBC, but likely due to PRECIS. Differences between modeled and observed temperature in the Andes may be caused by an inaccurate presentation of the model's topography.
- With respect to temperature,
  - the spatial pattern of the spatially interpolated observations and the RCM-results, match,
  - the RCM-results are closer to the observations than the GCM results,
  - the 25km-resolution data is closer to the observations than the 50km-resolution data,
  - the RCM systematically underestimates observations in sub-Andes and highlands,
  - the RCM-ECHAM4 properly estimates air temperature in the lowlands when comparing data points at the locations of the meteorological stations,
  - the GCM ECHAM4 underestimates the temperature in the lowlands and sub-Andes and overestimates the temperature in the highlands.
- With respect to precipitation,
  - the spatial pattern of the spatially interpolated observations and the RCM-results, do not match,
  - the GCM-results are closer to the observations than the RCM results,
  - the 50km-resolution data is a bit closer to the observations than the 25km-resolution data,
  - the RCM systematically overestimates precipitation in sub-Andes and highlands,
  - all modeled data is significantly different form observations,
  - the difference between the RCM-ECHAM4-results and observation is lowest in the lowlands,
  - the GCM ECHAM4 shows no systematic error and is much more similar to observations than the RCM.
- The RCM-results in the sub-Andes and highlands diverge systematically so much from the observations, that the results are so far invalid for both regions. In the lowlands on the other hand, temperature estimations are valid and precipitation is invalid. However, taking into account the low density of the meteorological stations and the large spatial variability of precipitation and the fact, that the difference between model and observation is not systematically, the RCM-results of precipitation in the lowlands may be considered reasonable.

Climate Change

- PRECIS models a stronger increase in air temperature in the highlands and Amazon. Spatial and temporal variability do not change. This tendency is confirmed by meteorological observations ranging from 1941-2004.
- PRECIS models a more intense precipitation cycle with more precipitation during the rain- and less precipitation during the dry season.
- Most of the annual net precipitation decrease occurs in the highlands and to some extent in the northern part of the lowlands (Amazon forest).
- The annual net increase of precipitation occurs in the southern part of the lowlands (dry forests) and to some extent in the northern part of the sub-Andes. Observed tendencies as presented in chapter 3.2.1 confirm modeled tendencies only with respect to drier conditions in the highlands. A drying in the northern part of Bolivia is not observed yet.
- The increase of temperature by 5°C and the simultaneous decrease of precipitation of by -36% during the dry months may imply severe impacts with respect to agricultural production, fire risk and ecosystem stability. An increase of precipitation by 45% during the rainy season implies an increasing risk of floods and erosion.

Follow-up research

- To locate the source of the bias, the author recommends (*i*) comparing the altitude used by PRECIS with a digital elevation model, (*ii*) improving the spatial observational data of precipitation with remote sensing data and (*iii*) reviewing the applicability of parameterization schemes for the Andes.
- If the altitude used in PRECIS shows no systematic bias and the applicability of the parameterization scheme is not given, then a different RCM with calibration options should be considered.
- If only lowland climate is of interest, a second evaluation with an improved precipitation map may be successful.
- In either case, to fully evaluate a RCM, more variables than temperature and precipitation should be observed. Circulation patterns such as the low level jet, the Bolivian high and the Chaco low (see chapter 1.3) should be examined. Also, the inner model consistency should be analyzed by comparing physically related variables.
- Due to the latitudinal precipitation gradient (see chapter 2.3), the author recommends to analyze the northern and southern part of the lowlands separately.

REFERENCES

Cox, P. M., R. A. Betts, C. B. Bunton, R. L. H. Essery, P. R. Rowntree and J. Smith, (1999) "The impact of new land surface physics on the GCM simulation of climate and climate sensitivity". *Clim. Dyn., 15:183-203.*

Fu, C., Wang, S., Xiong, Z., Gutowski, W. (2003) "Regional Climate Model Intercomparison Project for Asia (RMIP)". Submitted to *Bulletin of the American Meteorological Society*

Garreaud, R., (2003) "The Low-Level Jet off the West Coast of Subtropical South America: Structure and Variability". *Monthly weather review, Volume 133*

Garreaud, R.D., *et al*., (2008) "Present-day South American climate". *Paleogeogr. Palaeoclimatol. Palaeoecol., doi:10.1016/j.palaeo.2007.10.032*

Gordon, C., C. Cooper, C. A. Senior, H. Banks, J. M. Gregory, T. C. Johns, J. F. B. Mitchell and R. A. Wood, (2000) "The simulation of SST, sea ice extents and ocean heat transports in a version of the Hadley Centre coupled model without flux adjustments". *Clim. Dyn., 16:147-168*

Ibisch P.L. & G. Mérida (eds.) (2003). "Biodiversidad: La riqueza de Bolivia. Estado de conocimiento y conservación. Ministerio de Desarrollo Sostenible". *Editorial FAN, Santacruz de la Sierra – Bolivia.*

Jacob, D., Bärring, L., Christensen, O., et al., (2007) "An inter-comparison of regional climate models for Europe: model performance in present-day climate" *Climatic Change (2007) 81:31–52 DOI 10.1007/s10584-006-9213-4*

Jones, R.G., Noguer, M., Hassell, D.C., Hudson, D., Wilson, S.S., Jenkins, G.J. and Mitchell, J.F.B. (2004) "Generating high resolution climate change scenarios using PRECIS". *Met Office Hadley Centre, Exeter, UK, 40pp*

Killeen, T. J., A. Guerra, M. Calzada, L. Correa, V. Calderon, L. Soria, B. Quezada, and M. K. Steininger (2008) "Total historical land-use change in eastern Bolivia: Who, where, when, and how much?" *Ecology and Society* **13**(1): 36

Köhler, W., Schachtel, G., Voleske, P., (2002) „Biostatistik: Einführung in die Biometrie für Biologen und Agrarwissenschaftler". *3. Aufl., Springer Verlag, ISBN 3-540-42947-6, pp. 101*

Islam, N., Rafiuddin, M., Ahmed, A., Kolli, R., (2007) "Calibration of PRECIS in employing future scenarios in Bangladesh". *Int. J. Climatol, doi: 10.1002/joc.1559*

Marengo, J.A., Jones, R., Alves, L. Valverde, M. (2009) "Future change of temperature and precipitation extremes in South America as derived from the PRECIS regional climate modeling system". *Int. J. Climatol., DOI: 10.1002/joc.1863*

Molina, G., Estenssoro, A., Arce, R., Ocampo, M., Arauco, V., Sánchez, M. (2009) "La otra frontera – Usos alternativos de recursos naturales en Bolivia". *Informe temático sobre Desarrollo Humano del Programa de las Naciones Unidas para el Desarrollo (PNUD)*

Ontiverus, M. "Identificación de Índices de cambio climático en el territorio boliviano (En Base a R-ClimDex)". *Programma Nacional de Cambio Climático (PNCC), unpubl.*

Roads, J., S. Chen, S. Cocke, L. Druyan, M. Fulakeza, T. LaRow, P. Lonergan, J.-H. Qian, and S. Zebiak, (2003) "International Research Institute/Applied Research Centers (IRI/ARCs) regional model intercomparison over South America". *J. Geophys. Res., 108(D14), 4425, doi:10.1029/2002JD003201, 2003.*

Seth, A., Rauscher, S., Camargo, S., Qian, J., Pal, J. (2007) "RegCM3 regional climatologies for South America using reanalysis and ECHAM global model driving fields". *Clim Dyn (2007) 28:461–480, DOI 10.1007/s00382-006-0191-z*

Silvestri, G., Vera, C., Jacob, D., Pfeifer, S., Teichmann, C. (2009) "A high- resolution 43-year atmospheric hindcast for South America generated with the MPI regional model". *Clim Dyn (2009) 32:693–709, DOI 10.1007/s00382-008-0423-5*

Stull, R. (2000) "Meteorology for Scientists and Engineers". *Brooks/Cole*

Uppala., S.M., Kallberg, P., Simmons, A., Andrae, U. (2005) "The ERA-40 re-analysis". *Q. J. R. Meteorol. Soc. (2005), 131, pp. 2961–3012*

Veblen, T., Young, K., Orme, A. (2007) The Physical Geography of South America. *Oxford University Press*

Vera, C., Higgins, W., Amador, J., Ambrizzi, T., Garreaud, R., Gochis, D., Gutzler, D., Lettenmaier, D.,Marengo, J., Mechoso, C.R., Nogues-Paegle, J., Silva Diaz, P.L., Zhang, C. (2006) " Towards a unified view of the American Monsoon System". *J. Climate 19, 4977–5000*

ANNEX

Figures

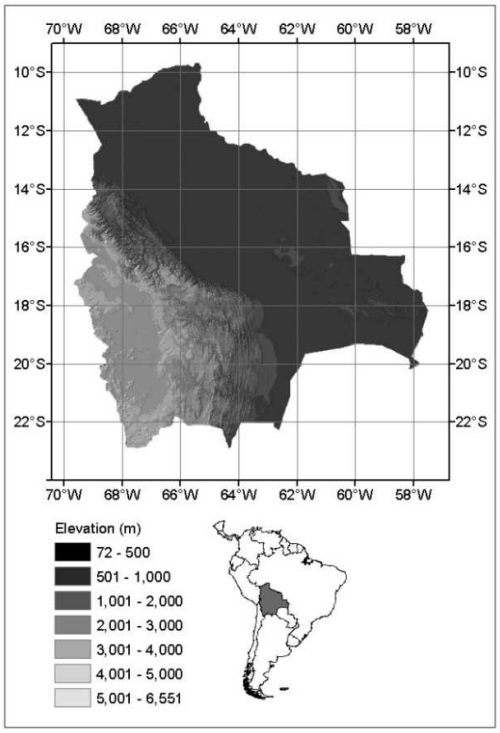

Figure 7 Surface elevation map of Bolivia (SRTM 90m Digital Elevation Model (DEM))

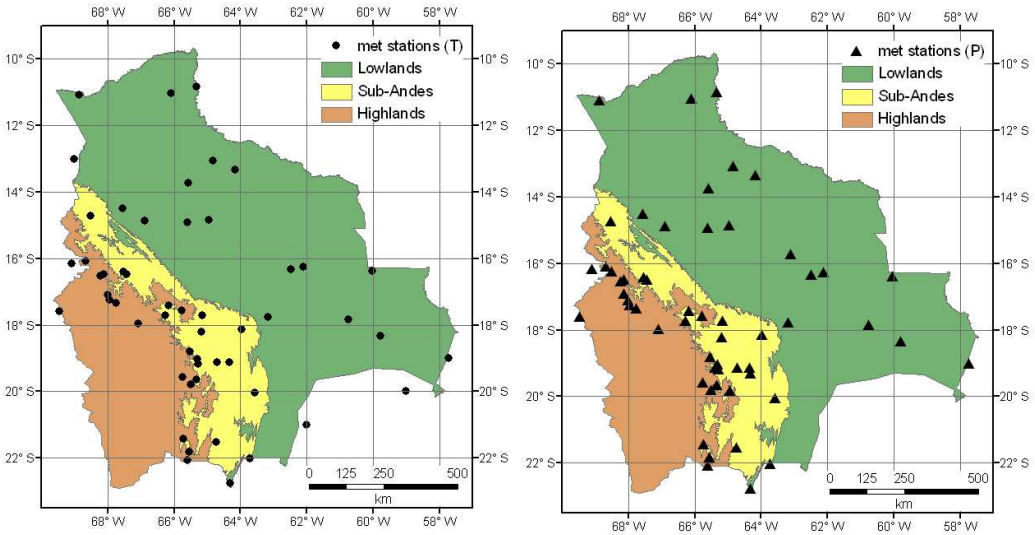

Figure 8 Distribution of meteorological stations for temperature (left) and precipitation (right) in lowlands, sub-Andes and highlands.

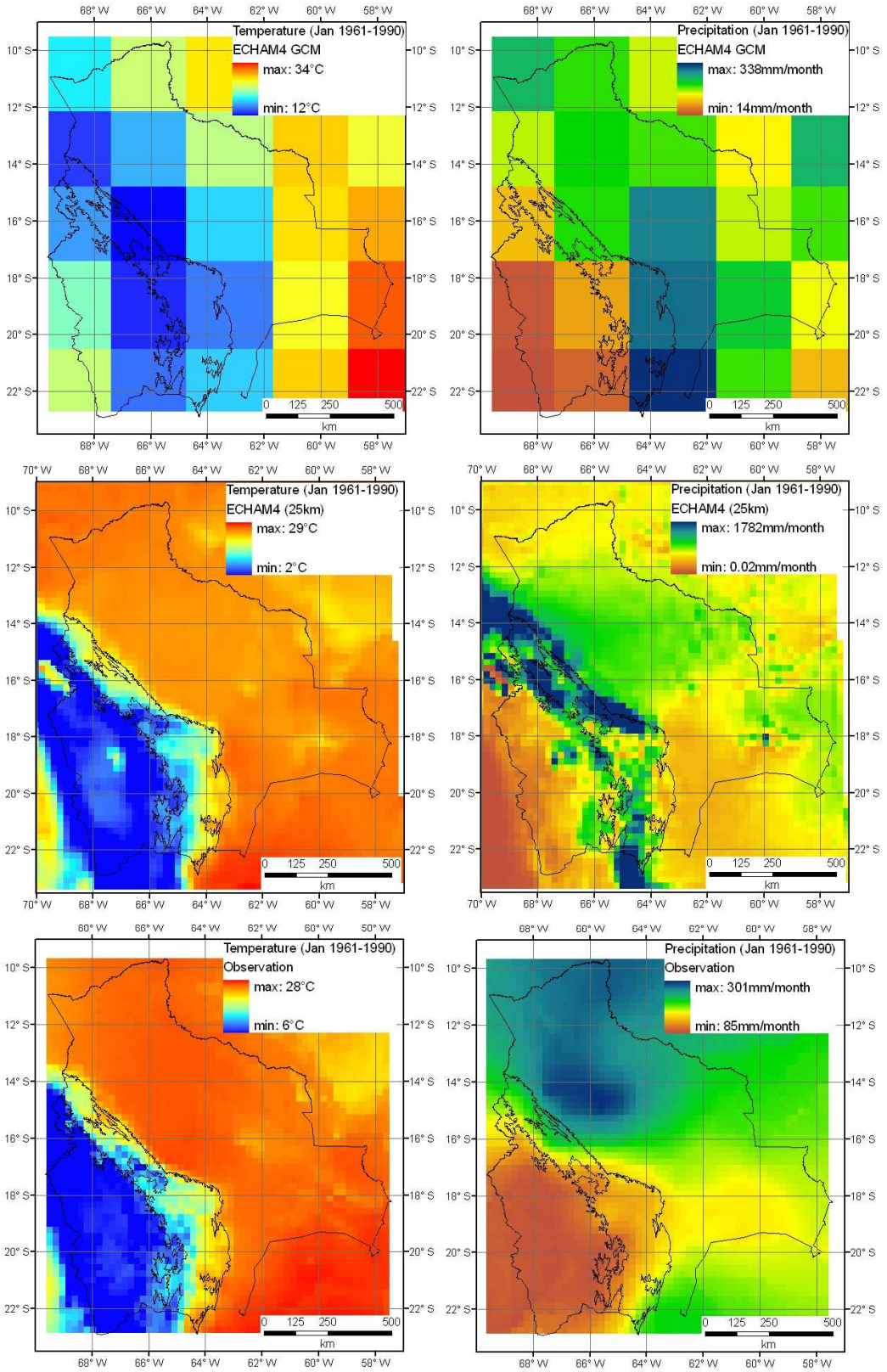

Figure 9 Temperature (left) and precipitation (right) of GCM (above), RCM (middle) and observation (below)

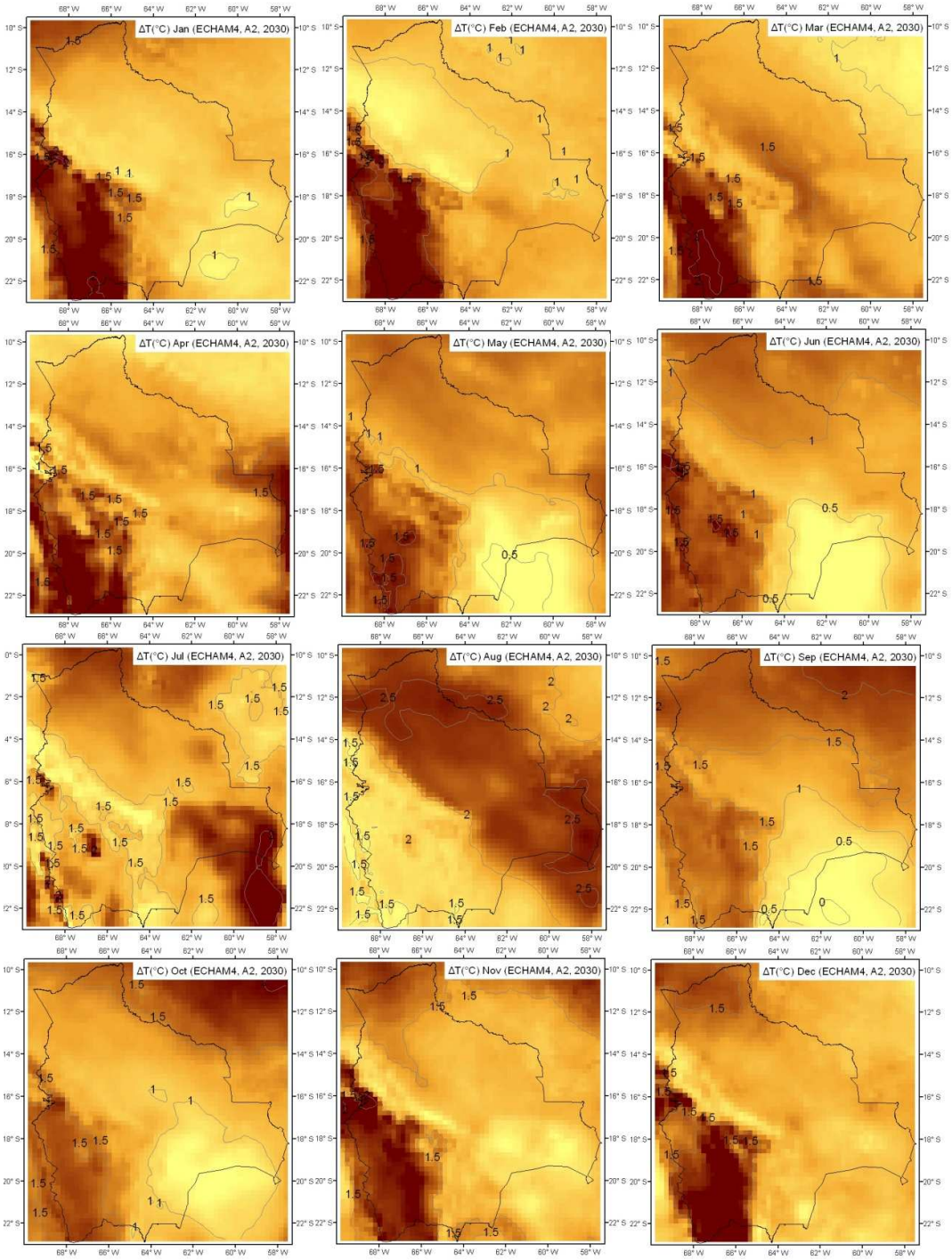

Figure 10 Change of mean monthly air temperature (°C) during 2001-2030 in reference to 1961-1990 (ECHAM4 A2)

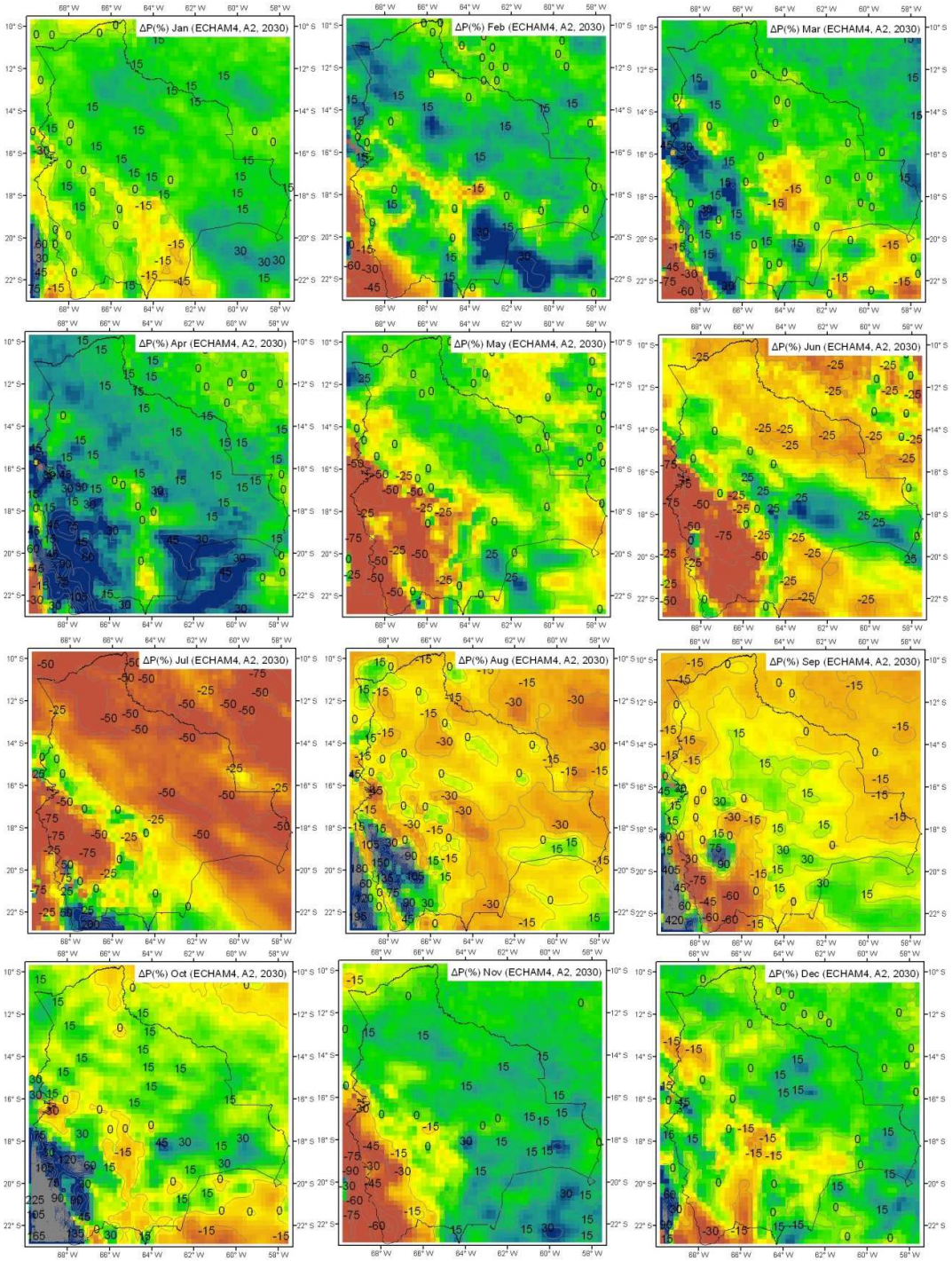

Figure 11 Change of mean monthly precipitation (%) during 2001-2030 in reference to 1961-1990 (ECHAM4 A2)

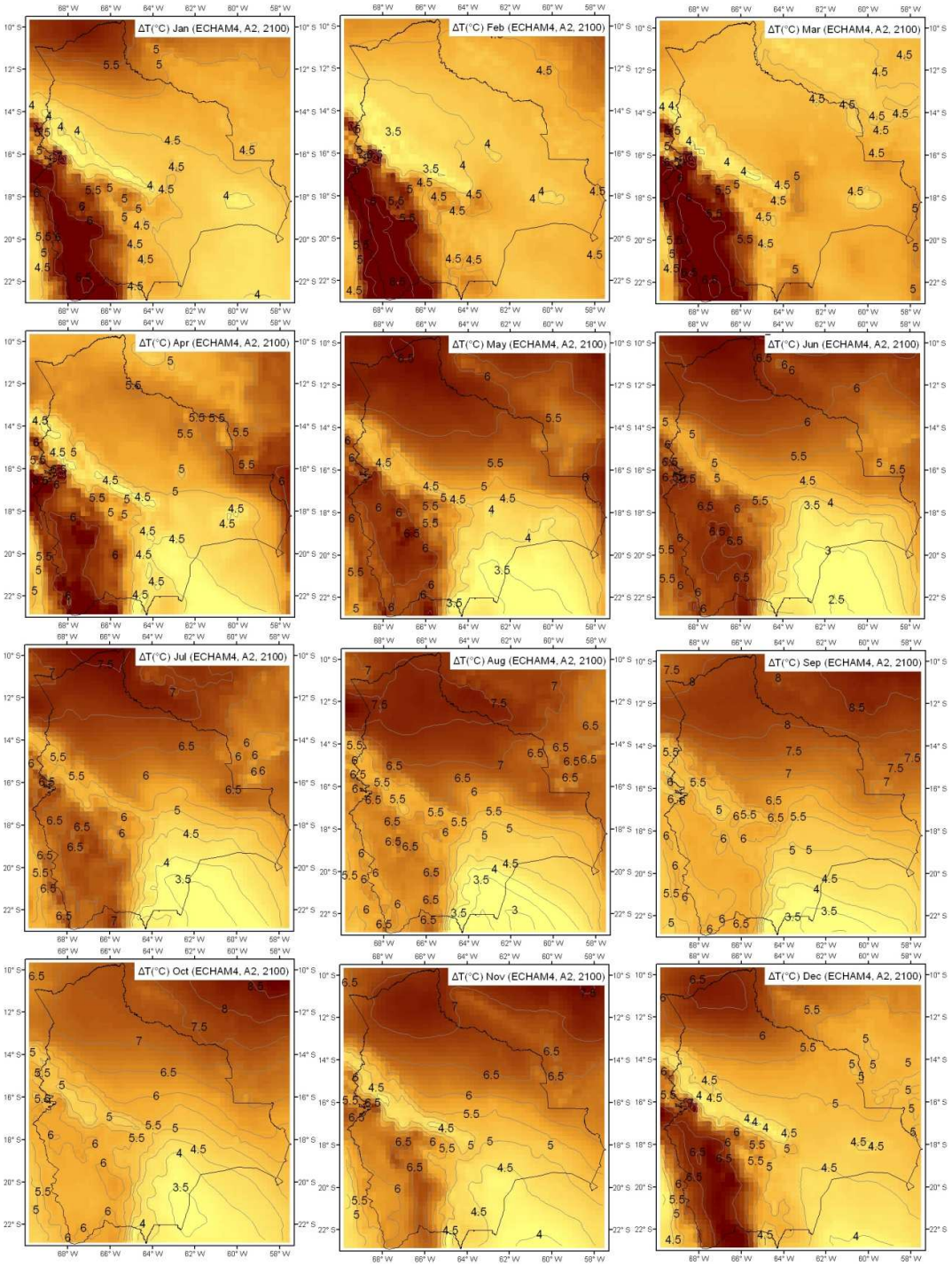

Figure 12 Change of mean monthly air temperature (°C) during 2071-2100 in reference to 1961-1990 (ECHAM4 A2)

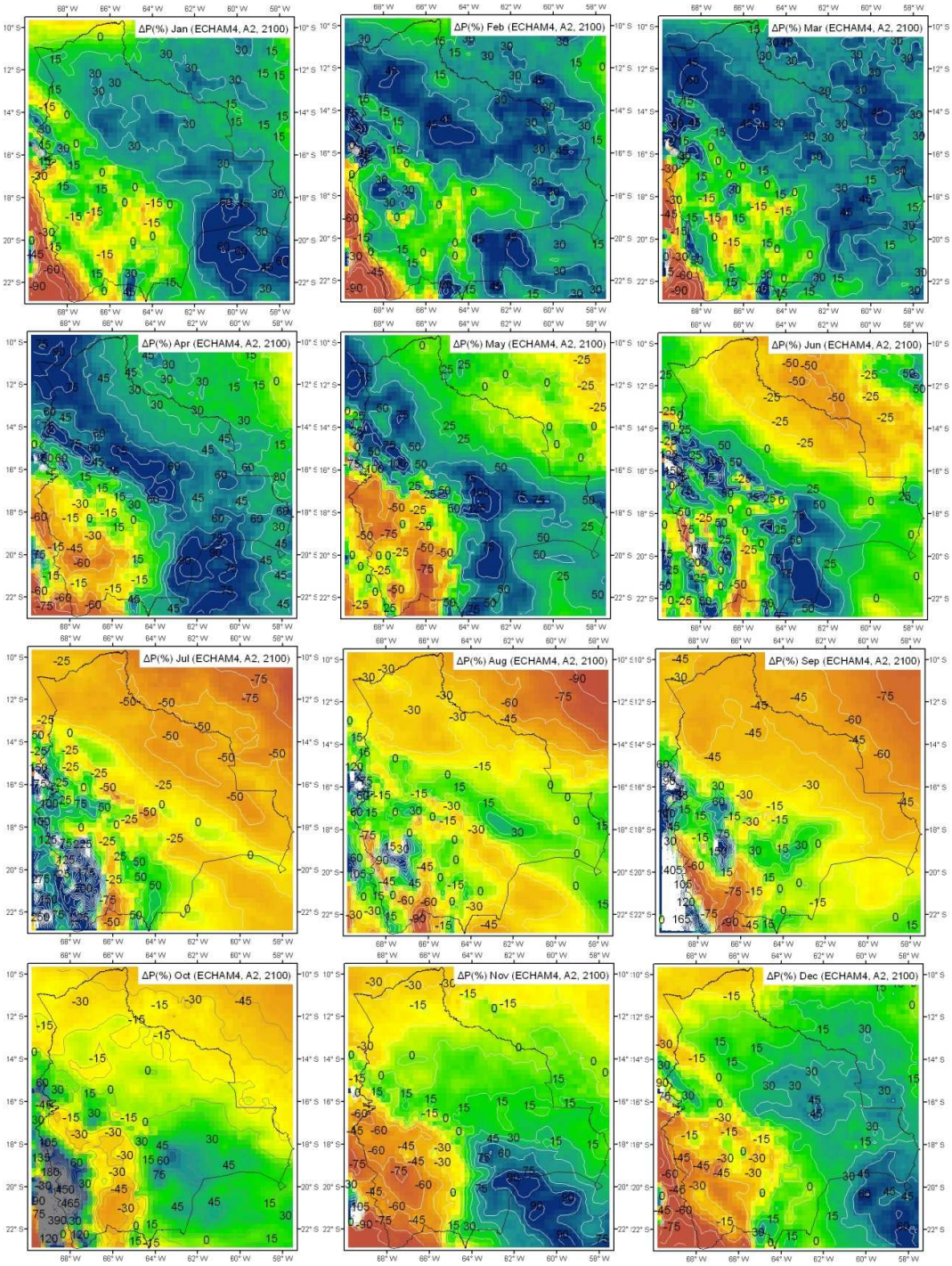

Figure 13 Change of mean monthly precipitation (%) during 2071-2100 in reference to 1961-1990 (ECHAM4 A2)

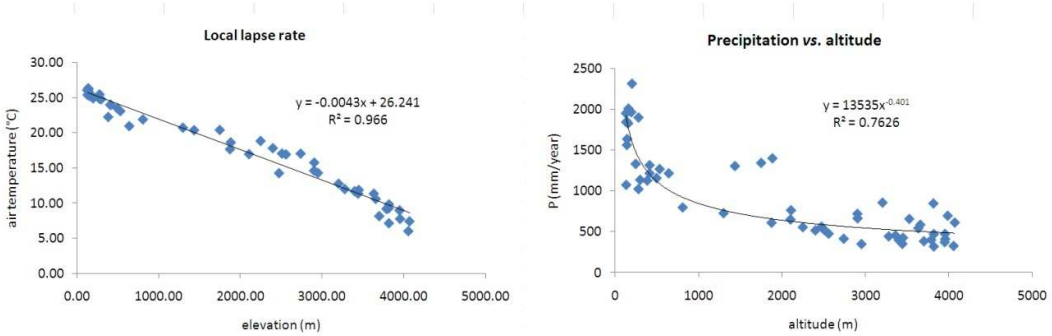

Figure 14 Temperature (left) and precipitation (right) plotted against altitude

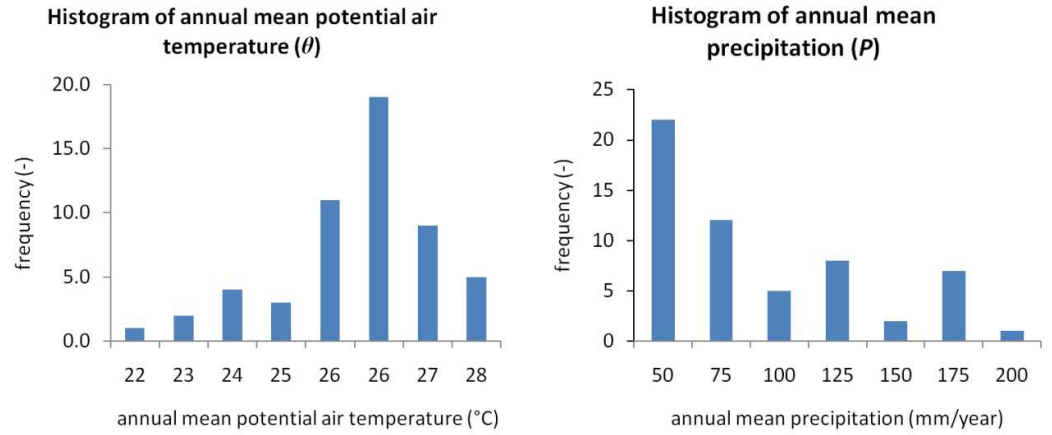

Figure 15 Histogram of annual mean potential air temperature (θ) (left) and annual mean precipitation (P) (right)

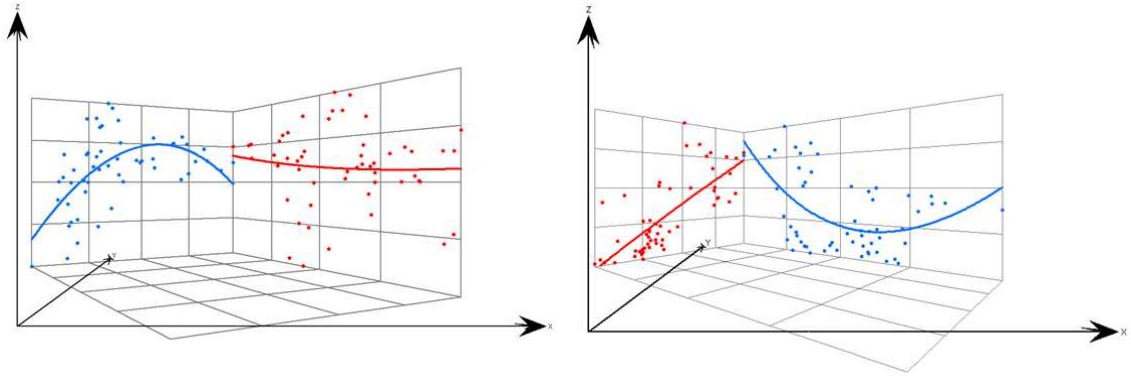

Figure 16 Trend analysis potential air temperature (left) and precipitation (right) (x = east, y = north, z = θ (left) $z = P$ (right), rotation angle = 30° and 50°)

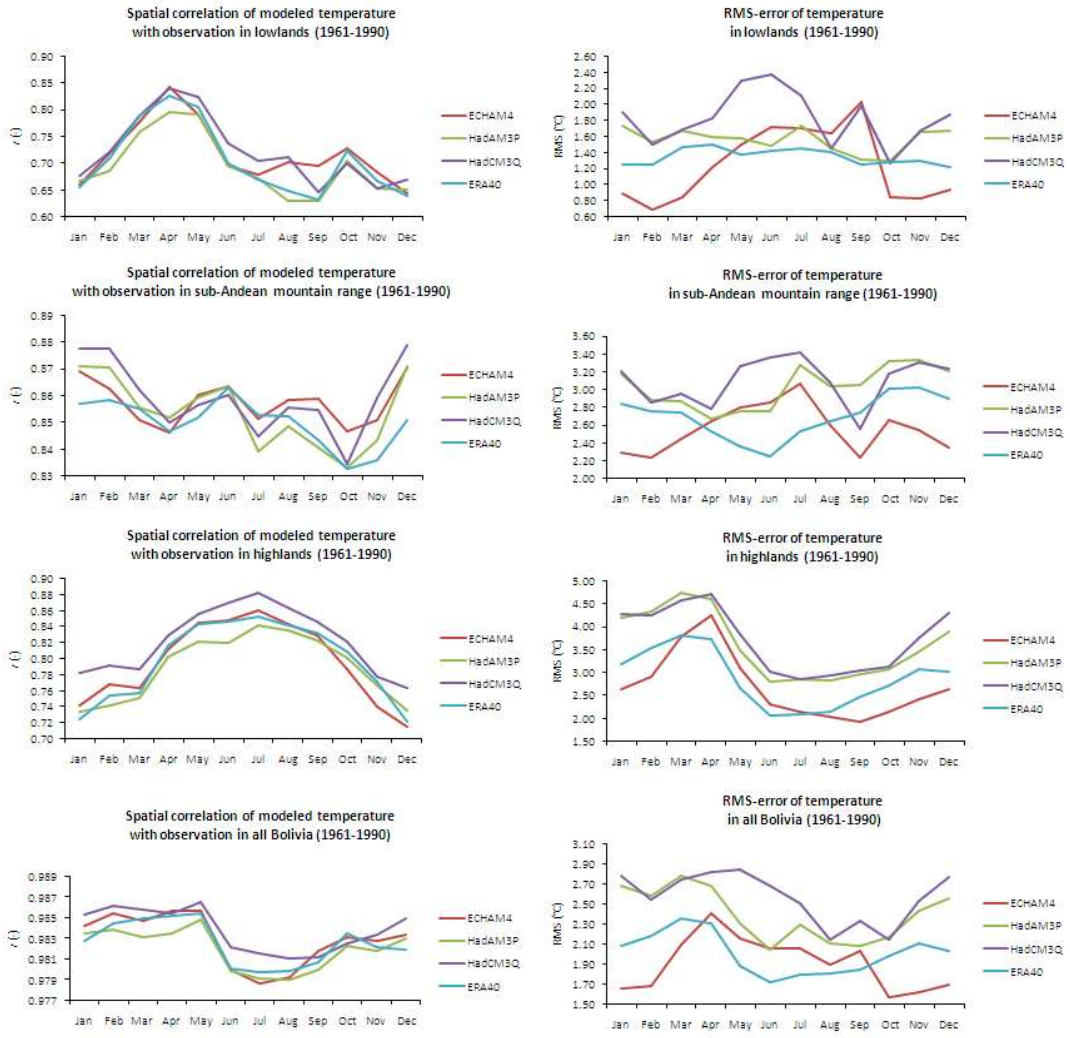

Figure 17 Spatial correlation (left) and RMS (right) of temperature

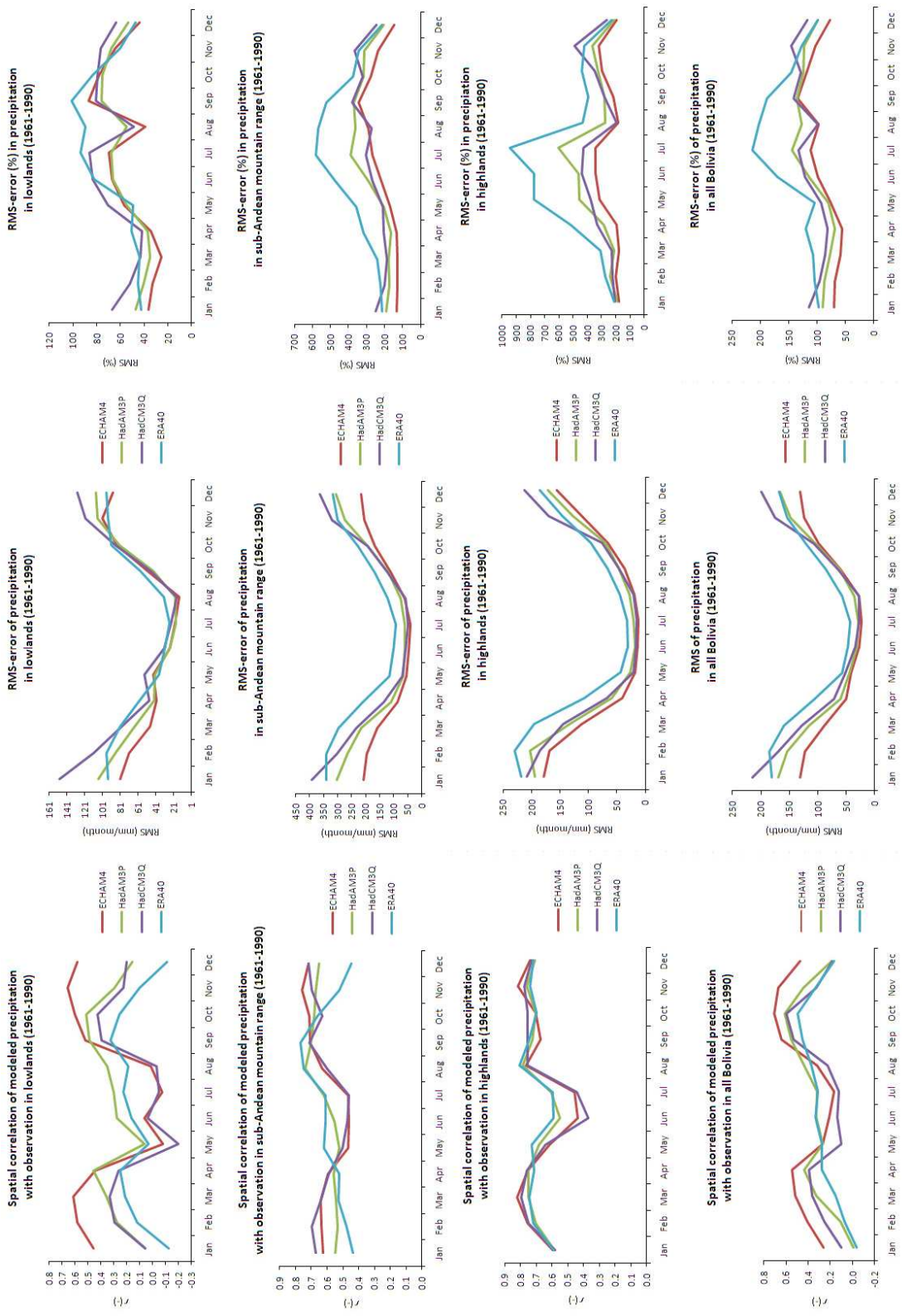

Figure 18 Spatial correlation (left) and RMS (right) of precipitation

Tables

Table 8 Examples of Regional Climate Modela applications in South America

Publication	Roads *et al.,* (2003)
Institute	University of California
RCM	RSM, FSUNRM, RCM, RegCM2
LBC	NCEP/NCAR reanalysis
Spatial resolution	50km
Slot	1997-1999
SRES	n.a.
Validation data	Land observations, (Xie and Arkin, 1997)
Model performance S. America	Temperature: n.a. Precipitation: Seasonal precipitation cycle present. 3 out of 4 RCM show stronger precipitation error in high- than lowlands in Bolivia.
Climate change S. America	n.a.
Publication	Seth *et al*., (2007)
Institute	Columbia University
RCM	RegCM3
LBC	ECHAM, NCEP/NCAR
Spatial resolution	80km
Slot	1950-2002
SRES	n.a.
Validation data	CMAP
Model performance S. America	Temperature: n.a. Precipitation: seasonal cycle present, dry bias in Amazon, wet bias in the south and east of Andes
Climate change S. America	n.a.
Publication	Silvestri *et al*., (2009)
Institute	CIMA/CONICET University of Buenos Aires, MPI
RCM	REMO
LBC	ERA40
Spatial resolution	0.5 degree
Slot	1958-2000
SRES	n.a.
Validation data	Meteorological observations (not spatially interpolated)
Model performance S. America	Temperature: Seasonal cycle present. Mainly overestimation, RMS 1.5°C Precipitation: Realistic temporal pattern of precipitation. Systematic overestimation of precipitation especially in the Andes
Climate change S. America	n.a.
Publication	Marengo *et al*., (2009)
Institute	CPTEC/INPE Brazil, UK Met Office Hadley Centre
RCM	PRECIS
LBC	HadCM3Q
Spatial resolution	0.55 degree

Slot	1961-1990; 2071-2100
SRES	A2, B2
Validation data	CRU
Model performance S. America	Temperature: Realistic spatial and temporal patterns. Underestimation, especially Andes
	Precipitation: Realistic spatial and temporal patterns. Overestimation during rainy season in Andes (DJF, SON). Underestimation of precipitation in Amazon (DJF, MAM)
Climate change S. America	Temperature: Amazon: +3 to +4°C (B2, 2100), Eastern Amazon: +8°C (A2, 2100)
	Precipitation: Eastern Amazon: -5 to -20% (B2, 2100), Eastern Amazon: -40% (A2, 2100)
Publication	Sörrensson *et al.,* (2009) (unpublished)
Institute	University of Buenos Aires
RCM	RCA3
LBC	ECHAM5, ERA40
Spatial resolution	0.5 degree
Slot	1980-1999, 2080-2099
SRES	A1B
Validation data	CRU
Model performance S. America	Temperature: underestimation in Andes, overestimation in some parts of lowlands
	Precipitation: overestimation in Andes
Climate change S. America	Temperature: maximum increase in the Amazon (6-7°C) and Andes
	Precipitation: decrease in southern Amazon and Bolivian Andes
Publication	Urrutia and Vuille (2009)
Institute	University of Massachusetts
RCM	PRECIS
LBC	HadCM3
Spatial resolution	0.44 degree
Slot	1961-1990, 2071-2100
SRES	A2, B2
Validation data	CRU
Model performance S. America	Cold and wet bias, especially in Andes
Climate change S. America	Temperature: strong increase in Bolivian Andes and Amazon (especially NE-Amazon)
	Precipitation: decrease in Bolivian Andes and Amazon (especially NE-Amazon)

Table 9 Characteristics of three SRES (A1B, A2, B2) (Nakicenovic *et al.*,2000)

Characteristics	**A1B**	**A2**	**B2**
Population growth	low	high	medium
GDP growth	very high	medium	medium
Energy use	very high	high	medium
Land-use changes	low	medium/high	medium
Resource availability	medium	low	medium
Pace and direction of technological change	rapid	slow	medium
Change favoring	balanced	regional	"dynamics as usual"

Table 10 Interpolation models

ID	variable	Method	Order of trend removal	Anisotropy	Angle direction	Searching neighborhood options	RMS	mean std.error
1	θ	kriging	none	no	no	default	0.957	1.244
2	θ	kriging	2nd	no	no	default	0.940	1.160
3	θ	kriging	2nd	yes	84.0	default	0.918	1.156
4	T	co-kriging (z)	none	no	no	default	2.059	3.645
1	P	kriging	none	no	no	default	15.32	21.92
2	P	kriging	1st	no	no	default	16.00	19.04
3	P	kriging	2nd	no	no	default	18.74	16.63
4	P	kriging	1st	yes	123.7	default	15.70	17.59
5	P	kriging	2nd	yes	127.0	default	18.47	16.05
6	P	co-kriging (z)	none	no	no	default	15.52	21.65
7	P	co-kriging (z)	1st	no	no	default	16.21	20.59
8	P	co-kriging (z)	2nd	no	no	default	26.80	25.26
9	P	co-kriging (z)	2nd	yes	137.6	default	28.92	25.68

Table 11 Interpolation models for temperature using monthly data

	m1*		m2**		Which model performs better?	
	RMS error	mean std.error	RMS error	mean std.error	RMS error	mean std.error
JAN	0.79	1.09	0.82	1.06	m1	m2
FEB	0.77	1.09	0.81	1.04	m1	m2
MAR	0.78	1.05	0.82	1.01	m1	m2
APR	0.96	1.23	1.00	1.17	m1	m2
MAY	1.31	1.65	1.16	1.39	m2	m2
JUN	1.68	1.91	1.51	1.60	m2	m2
JUL	1.71	1.90	1.57	1.55	m2	m2
AUG	1.55	1.78	1.38	1.44	m2	m2
SEP	1.38	1.62	1.21	1.29	m2	m2
OCT	1.09	1.34	1.05	1.24	m2	m2
NOV	1.00	1.31	1.02	1.27	m1	m2
DEC	0.86	1.18	0.92	1.08	m1	m2

*m1= ordinary kriging using default options,
**m2 = ordinary kriging with second order trend removal

Table 12 Interpolation model for precipitation using monthly data

	m6			
	RMS error (mm/month)	mean std.error	mean OBS (mm/month)	RMS (%)
JAN	30.20	42.91	165.80	18.21
FEB	31.71	40.67	147.89	21.44
MAR	29.62	33.52	124.50	23.79
APR	19.84	23.71	65.79	30.15
MAY	15.64	18.11	36.26	43.13
JUN	15.39	15.94	18.41	83.58
JUL	11.70	12.57	14.18	82.53
AUG	13.65	18.45	22.09	61.80
SEP	13.38	18.71	36.44	36.72
OCT	13.56	21.60	64.41	21.05
NOV	20.00	27.53	92.55	21.61
DEC	26.64	34.98	142.41	18.71
			mean RMS (%)	**38.56**

Table 13 Comparison of the RCM-ECHAM4 with observations at the locations of meteorological stations.

ID	Validation			All Bolivia	Lowlands	Sub-Andes	Highlands
a	GCM ECHAM4 vs. OBS	Temp.	RMS (°C)	7.24	8.59	6.80	5.50
			r	0.55	0.35	0.70	0.33
			t_{Vers}	9.801	14.881	17.531	5.042
			t_{Tab} (α = 0.05)	1.961	1.970	1.970	1.970
		Prec.	RMS (mm/month)	63	74	75	24
			RMS (%)	79%	58%	122%	57%
			r	0.73	0.67	0.62	0.86
			t_{Vers}	0.445	0.551	1.590	2.586
			t_{Tab} (α = 0.05)	1.963	1.970	1.970	1.970
b	ECHAM4 (25km) vs. OBS	Temp.	RMS (°C)	3.75	1.42	4.86	5.50
			r	0.91	0.85	0.79	0.43
			t_{Vers}	4.423	1.039	11.923	4.508
			t_{Tab} (α = 0.05)	1.961	1.970	1.970	1.970
		Prec.	RMS (mm/month)	119	80	158	109
			RMS (%)	150%	62%	256%	252%
			r	0.73	0.83	0.88	0.74
			t_{Vers}	10.183	2.972	8.955	6.551
			t_{Tab} (α = 0.05)	1.963	1.970	1.970	1.970
c	ERA40 (50km) vs. OBS	Temp.	RMS (°C)	3.80	1.67	5.06	4.42
			r	0.93	0.86	0.79	0.53
			t_{Vers}	6.177	5.091	14.994	6.647
			t_{Tab} (α = 0.05)	1.961	1.970	1.970	1.970
		Prec.	RMS (mm/month)	157	65	233	136
			RMS (%)	199%	50%	376%	315%
			r	0.51	0.76	0.69	0.77
			t_{Vers}	14.273	2.620	12.115	10.182
			t_{Tab} (α = 0.05)	1.963	1.970	1.970	1.970
d	RCM vs. GCM ECHAM4	Temp.	RMS (°C)	6.75	8.32	3.63	6.60
			r	0.61	0.41	0.67	0.39
			t_{Vers}	4.455	14.101	4.934	8.189
			t_{Tab} (α = 0.05)	1.961	1.970	1.970	1.970
		Prec.	RMS (mm/month)	129	114	144	132
			RMS (%)	163%	88%	232%	307%
			r	0.60	0.69	0.54	0.74
			t_{Vers}	9.371	2.430	7.282	7.779
			t_{Tab} (α = 0.05)	1.963	1.970	1.970	1.970

Table 14 RCM Temperature and Precipitation bias of 31 applications worldwide

RCM	Domain	Temp. bias (°C) (absolute)	Prec. bias (%) (absolute)	Source
HIRHAM	Europe	0.95	13	Jacob *et al*., (2007)
HIRHAM25	Europe	0.85	15	Jacob *et al*., (2007)
HIRHAM12	Europe	0.90	17	Jacob *et al*., (2007)
CHRM	Europe	0.65	25	Jacob *et al*., (2007)
CLM	Europe	1.00	27	Jacob *et al*., (2007)
HadRM3H	Europe	1.35	16	Jacob *et al*., (2007)
RegCM	Europe	0.75	19	Jacob *et al*., (2007)
RACMO	Europe	1.20	16	Jacob *et al*., (2007)
HIRHAM.no	Europe	1.05	19	Jacob *et al*., (2007)
REMO	Europe	1.40	20	Jacob *et al*., (2007)
RCAO	Europe	1.45	23	Jacob *et al*., (2007)
RCAO22	Europe	1.30	26	Jacob *et al*., (2007)
PROMES	Europe	0.85	14	Jacob *et al*., (2007)
HadAM3H	Europe	0.85	17	Jacob *et al*., (2007)
ARPEGE	Europe	0.60	19	Jacob *et al*., (2007)
RIEMS	Asia	2.26	10	Fu *et al*., (2003)
CCAM	Asia	1.37	25	Fu *et al*., (2003)
DARLAM	Asia	0.85	25	Fu *et al*., (2003)
SNU RCM	Asia	3.13	29	Fu *et al*., (2003)
RegCM	Asia	3.08	16	Fu *et al*., (2003)
RegCM2	Asia	2.58	25	Fu *et al*., (2003)
RegCM3	Asia	2.85	22	Fu *et al*., (2003)
ALT MM5/LSM	Asia	2.99	39	Fu *et al*., (2003)
MRI	Asia	2.90	23	Fu *et al*., (2003)
RSM	S. America	-	2	Roads *et al*., (2003)
FSUNRSM	S. America	-	13	Roads *et al*., (2003)
RegCM2	S. America	-	15	Roads *et al*., (2003)
RCM	S. America	-	23	Roads *et al*., (2003)
PRECIS	Bangladesh	2.68	28	Nazrul *et al.,* (2007)
PRECIS	India	3.63	54	Kumar *et al*., (2006)
PRECIS	S. Africa	0.96	26	Hudson and Jones (2002)
Statistics	mean	1.65	21	
	min	0.60	2.44	
	max	3.63	54	
	Std. dev.	0.95	9	